Seismic monitoring of soft-rock landslides: the Super-Sauze and Valoria case studies

Alice Tonnellier, Agnès Helmstetter, Jean-Philippe Malet, Jean Schmittbuhl, Alessandro Corsini, Manfred Joswig

Geophysical Journal International

Geophys. J. Int. (2013) **193,** 1515–1536
Advance Access publication 2013 March 08

doi: 10.1093/gji/ggt039

Seismic monitoring of soft-rock landslides: the Super-Sauze and Valoria case studies

Alice Tonnellier,[1] Agnès Helmstetter,[2] Jean-Philippe Malet,[1] Jean Schmittbuhl,[1] Alessandro Corsini[3] and Manfred Joswig[4]

[1] *Institut de Physique du Globe de Strasbourg, CNRS UMR* 7516*, EOST, Université de Strasbourg, France. E-mail: alice.tonnellier@unistra.fr*
[2] *ISTerre, Université de Grenoble* 1*, CNRS, France*
[3] *Dipartimento di Scienze della Terra di Modena e Reggio Emilia, University of Modena, Italy*
[4] *Institut für Geophysik, University of Stuttgart, Germany*

Accepted 2013 January 28. Received 2013 January 23; in original form 2012 August 16

SUMMARY

This work focuses on the characterization of seismic sources observed in clay–shale landslides. Two landslides are considered: Super-Sauze (France) and Valoria (Italy). The two landslides are developed in reworked clay–shales but differ in terms of dimensions and displacement rates. Thousands of seismic signals have been identified by a small seismic array in spite of the high-seismic attenuation of the material. Several detection methods are tested. A semi-automatic detection method is validated by the comparison with a manual detection. Seismic signals are classified in three groups based on the frequency content, the apparent velocity and the differentiation of *P* and *S* waves. It is supposed that the first group of seismic signals is associated to shearing or fracture events within the landslide bodies, while the second group may correspond to rockfalls or debris flows. A last group corresponds to external earthquakes. Seismic sources are located with an automatic beam-forming location method. Sources are clustered in several parts of the landslide in agreement with geomorphological observations. We found that the rate of rockfall and fracture events increases after periods of heavy rainfall or snowmelt. The rate of microseismicity and rockfall activity is also positively correlated with landslide displacement rates. External earthquakes did not influence the microseismic activity or the landslide movement, probably because the earthquake ground motion was too weak to trigger landslide events during the observation periods.

Key words: Image processing; Geomorphology; Early warning.

1 INTRODUCTION

Landslide failures may seriously damage the human and environmental resources of a region. However, it is still uneasy to forecast the evolution of a landslide because it depends both on its dynamics and on external triggering events, such as earthquakes and rainfall (Guzzetti *et al.* 2007). To better understand these processes, passive seismic monitoring techniques have been developed since the 1960s, in order to detect possible seismic signals triggered by the slope dynamics (Cadman & Goodman 1967; Novosad *et al.* 1977). It consists generally in identifying seismic sources induced by the slope movement using seismic sensors. In the case of slope failures, these seismic signals can be induced by several mechanisms such as material bending and shearing, material compression, surface fissure opening, slip at the bedrock interface, rockfalls and clast falls or debris flows. Passive seismic monitoring has been carried out on very diverse geological contexts and for very different objectives, and the number of studies has increased in the last decades. Some studies record the microseismic activity within landslides (Roth *et al.* 2005; Brückl & Mertl 2006; Spillmann *et al.* 2007; Helmstetter & Garambois 2010), rock cliffs (Amitrano *et al.* 2005; Mourot 2008; Senfaute *et al.* 2009; Lévy *et al.* 2011), glaciers (Stuart *et al.* 2005; Roux *et al.* 2008), mines and sinkholes (Ge 2005; Wust-Bloch & Joswig 2006; Wang & Ge 2007; Yang *et al.* 2007), in order to monitor the progressive damage and deformation of unstable slopes. In some cases, seismic signals have been detected before failure phenomena (Amitrano *et al.* 2005; Wang & Ge 2007; Yang *et al.* 2007; Mourot 2008). In other cases, seismic sensors are used to characterize the volume and propagation velocity of slope failures such as rockfalls or rockslides (Deparis *et al.* 2008; Dammeier *et al.* 2011; Hibert *et al.* 2011), snow and rock–ice avalanches (Kishimura & Izumi 1997; Suriñach *et al.* 2000; Suriñach *et al.* 2001; Schneider *et al.* 2010; Lacroix *et al.* 2012), debris flows (Arattano & Deganutti 2001; Marchi *et al.* 2001; Huang *et al.* 2004; Arattano & Marchi 2005; Burtin *et al.* 2009) and volcanic landslides (Esposito *et al.* 2006; De Angelis *et al.* 2007; Cole *et al.* 2009;

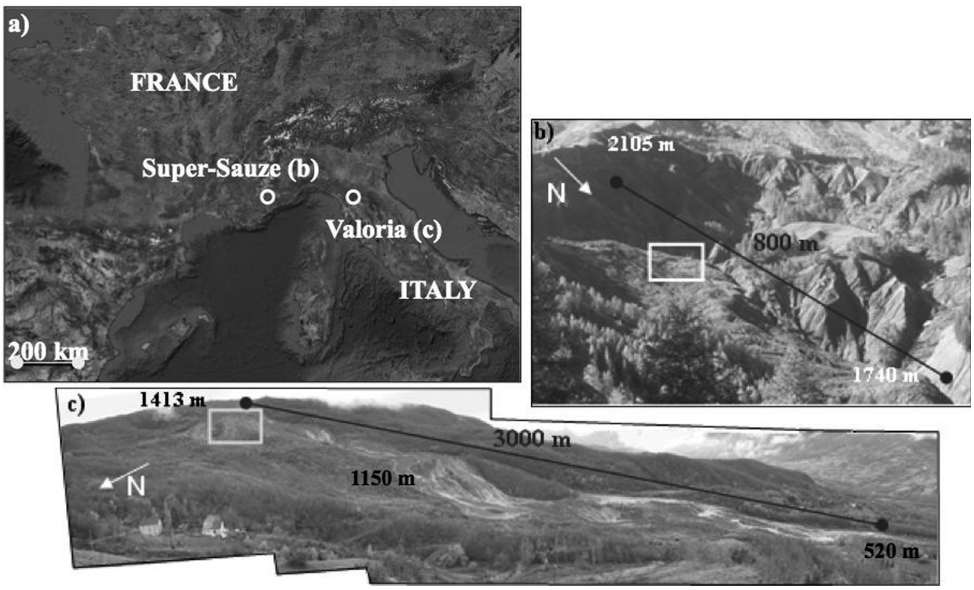

Figure 1. Location of the studied landslides: (a) global view, (b) zoom at the Super-Sauze landslide (Rothmund October 2009, personal communication) and (c) zoom at the Valoria landslide (Ronchetti 2009, personal communication). The frames on Figs 1b and 1c indicate the location of the seismic arrays.

Zobin *et al.* 2009). Other studies evaluate the correlation between seismic signals and external events such as rainfall (Rouse *et al.* 1991; Walter & Joswig 2008, 2009; Helmstetter & Garambois 2010; Hibert *et al.* 2011; Lacroix *et al.* 2012). Few analyses were carried out to characterize the seismic signals observed within soft-rock or sediment-type slope movements (Amitrano *et al.* 2007; Méric *et al.* 2007; Walter & Joswig 2008, 2009; Walter *et al.* 2009; Gomberg *et al.* 2011). Seismic signals are difficult to identify because of the spatial heterogeneity and the high saturation (close to 100 per cent) of the soft muddy materials (such as clays, shales and marls). This causes a high attenuation of the signal and a low signal-to-noise ratio. Recent monitoring techniques have been developed to compensate for these difficulties. They consist in detecting signals by analysing the variation with time of the signal frequency content (spectrogram). Joswig (2008) introduced 'nanoseismic monitoring' to analyse very weak signals in small areas. This technique has been used for the analysis of sinkholes failures (Wust-Bloch & Joswig 2006), cliff collapses (Lévy *et al.* 2011) and for exploratory analyses on muddy landslides (Walter & Joswig 2008, 2009; Walter *et al.* 2009). To reduce the time dedicated to manual picking of a large number of signals, semi-automatic techniques have been developed for the detection, classification and location, of seismic signals, in particular for rock slopes (Spillmann *et al.* 2007; Helmstetter & Garambois 2010; Lacroix & Helmstetter 2011).

Seismic monitoring can be used as a non-invasive investigation tool, in complement to displacement monitoring (e.g. GPS, extensometers, cameras. . .) or local borehole instrumentation. Unlike punctual displacement measures or boreholes, it can provide a global overview of landslide movements and deformations. Seismic monitoring offers several applications for slope instabilities. Analysing seismic noise can help in characterizing the landslide structure (Méric *et al.* 2007) and its evolution with time (Mainsant *et al.* 2012). Recording seismic signals produced by the slope movement can provide relevant information on the dynamics of the slide and may allow the identification of precursors. Seismic signals can be classified (rockfalls, fracture events), characterized (frequency content, magnitude, volume and propagation velocity of rockfalls or debris flows), and located. In the case of weak seismic signals, the detection of slope failures is made difficult by the presence of external acoustic noises (rainfall, water stream, wind, electrical equipment and field workers among others).

In this work, we focus on the detection of seismic signals possibly induced by the dynamics of the Super-Sauze (Southeast Alps, France) and Valoria (Northern Apennines, Italy) muddy landslides (Fig. 1). We focused on these landslides because they are very well instrumented and because there have been yet very few seismic monitoring studies on muddy landslides in the literature. Also, both landslides exhibit a complex dynamics, with frequent reactivation phases controlled by hydrometeorological triggers (Malet 2003; Ronchetti 2008). It is therefore interesting to analyse the microseismic activity and the kinematics regime observed during these reactivations phases. In the future, this might help us to predict such reactivations from microseismic activity monitoring.

The objective of this manuscript is to propose a typology of seismic signals, and to analyse their spatial and temporal distributions in relation to the landslide kinematics and other environmental factors. Three specific periods, characterized by different surface displacement rates, are analysed: a period of low-surface displacement rates ($<0.01\,\mathrm{m\,d^{-1}}$) at the Super-Sauze landslide during 2 weeks in 2009 October, a period of moderate surface displacement rates ($<0.10\,\mathrm{m\,d^{-1}}$) at the Super-Sauze landslide during 4 weeks in 2010 May and a period of very fast displacement ($>0.10\,\mathrm{m\,d^{-1}}$) at the Valoria landslide during 1 week in 2009 November, marked by an important acceleration of the slide.

The two landslides are essentially composed of highly attenuating soft-clay material and characterized by different kinematic regimes with the succession of acceleration and deceleration periods. For this analysis, we installed seismic acquisition systems on the upper parts of the landslides, in order to obtain a continuous seismic monitoring. We used spectrogram analyses to process the seismic observations, as proposed by Walter & Joswig (2008, 2009) and Walter & Joswig (2009). We applied the semi-automatic detection method proposed by Helmstetter & Garambois (2010) and went further on by locating the seismic signals detected on both landslides with the beam-forming location approach of Lacroix & Helmstetter (2011).

Table 1. Characteristic of the Super-Sauze and Valoria landslides.

Site	Super-Sauze	Valoria
Triggering/reactivation date	1960s	1950s
Geology	clay–shale	flysch, clay–shale
Dimensions (length, width, thickness)	800 m × 130 m × 15 m	3500 m × 300 m × 20 m
Estimated volume	550 000 m^3	32 000 000 m^3
Range of displacement rates	0.0001 m d^{-1} to 0.4 m d^{-1}	0.001 m d^{-1} to 0.65 m d^{-1}

We first present the characteristics of the two landslides and detail the different seismic acquisition systems. Detection and location methods are then detailed. The characteristics of seismic signals and their source mechanisms are then discussed. Finally, we compare microseismic activity and the observed displacement rates with external triggering factors such as earthquakes, rainfall and changes in groundwater levels.

2 CHARACTERISTICS OF THE TWO LANDSLIDE CASE STUDIES

The Super-Sauze and Valoria landslides are developed in clay–shale formation and are characterized by a complex kinematic pattern controlled by hydrometeorological conditions, and thus varying with the seasons (Table 1).

2.1 Characteristics of the Super-Sauze landslide

The Super-Sauze landslide (Fig. 1b) is located in the Southern French Alps (Barcelonnette Basin), in the upstream part of the Sauze torrential catchment. It was triggered in the 1960s when several rockslides occurred on a rocky slope composed of Callovo–Oxfordian black marls. After a period of mechanical weathering of the accumulated blocks, a slide has progressively developed in the 1980s with the downstream propagation of the reworked black marls in the torrential channel. Currently, the moving mass has a volume estimated at 550 000 m^3 and has an average thickness of 15 m (Travelletti & Malet 2012). The landslide has a length of nearly 800 m and a maximal width of 130 m, and develops between an elevation of 2105 m at the crown and 1705 m at the toe. The structure of the landslide consists of a complex geometry with the presence of steep gullies and crests (Travelletti & Malet 2012). The landslide material is composed of a silty–clayey matrix with the presence of unaltered rigid blocks of marls and limestones. The landslide has been extensively studied and monitored from the 1990s. Since 2007, it is part of the French Observatory on Landslide (omiv.osug.fr), which aims at acquiring and distributing multiparameter observations on different types of landslides through geomorphologic, geologic, hydrologic, geophysical and seismological long-term monitoring. The surface displacement is monitored through GPS campaigns (Malet *et al.* 2002) and permanent GPS monitoring (Déprez *et al.* 2011), extensometry (Malet *et al.* 2002), terrestrial laser scanners (Travelletti *et al.* 2008) and correlation of terrestrial photographs (Travelletti *et al.* 2011). The displacement field is very variable in space and time. Displacement rates can reach up to 0.40 m d^{-1} in spring in the most active part in the upper area of the landslide and decrease to 0.01 m d^{-1} downhill at the toe. In the upper part, the displacement is more complex with the presence of two stable crests (which we named for this paper '*in situ* crest' and 'boundary crest' in Fig. 2a; Malet 2003). This complex topography creates differential lateral movements between slowly moving and more rapidly moving compartments. A vertical three-layer structure has been proposed (Travelletti & Malet 2012) based on geological, hydrogeological, geotechnical and geophysical observations (Weber 1994; Malet 2003). The first superficial layer has a 5–9-m thickness and is bounded at its bottom by a shear surface that has been identified in borehole cores (Malet 2003). Below, this slip surface, a second layer, of 5–10-m thickness, is very compacted and characterized by very low displacements; the interface with the bedrock corresponds also to a slip surface identified in borehole cores (Malet 2003). The third layer corresponds to the stable intact black marl substratum. Seismic tomography studies have shown that the landslide structure is defined by P and S seismic wave velocity increasing progressively from $V_P = 600\,m\,s^{-1}$ and $V_S < 300\,m\,s^{-1}$, at the top, to V_P comprised between 2100 and 2400 m s^{-1} and $V_S > 550\,m\,s^{-1}$ in the bedrock (Grandjean *et al.* 2006; Amitrano *et al.* 2007; Méric *et al.* 2007; Walter & Joswig 2009). Tomography acquisitions were carried on in 2010 July, in order to propose a higher resolution structural model of the landslide in the direct vicinity of the seismic observation systems. The tomography acquisition (grey colour dot lines in Fig. 2a) consisted of two profiles of 80–90-m length crossing the landslide from the east to the west. Forty 14-Hz sensors were installed every 2 m and sources were located every 4 m. Data was acquired at 2000 Hz in order to observe the discontinuities of the first metres of sediments. Two models were obtained that indicate a first layer sliding on the bedrock. P-wave velocity of the upper and the lower profiles are presented in Fig. 3. They vary between 350 and 700 m s^{-1} in the first layer and between 2200 and 2300 m s^{-1} in the second layer and are significantly higher in the lower profile. The sliding layer is 5–10-m thick in the central part of the profile, from the upper to the lower region respectively, where the accumulation of sediments is higher. A stable crest is identified between the sliding layer and the bedrock, which is labelled as the 'boundary crest' in Fig. 2(a) and marked by the black arrow.

In 2008, small seismic arrays were deployed across the landslide during several 15-d acquisition periods to detect seismic events (Walter *et al.* 2009). The objective of these studies was to investigate the possibility of monitoring seismic signals for such types of landslides. The authors proved that it was possible to detect weak seismic signals of magnitude $M_L \sim -2$ in soft clays, in spite of the high attenuation of the material. They provided an overview of the spatial distribution of the seismic sources and concluded that most of them were located in the upper part of the landslide and were associated to rockfall events, essentially triggered from the main scarp, and to the opening of fissures measured by extensometers (Walter *et al.* 2011).

2.2 Characteristics of the Valoria landslide

The Valoria landslide (Fig. 1c) is located in the Northern Apennines (Italy), in the upper Dolo River (tributary of the Secchia River) basin. It has been reactivated seven times since the 1950s. This complex landslide is affected by deep-seated mass movements from the Late glacial period (Garberi *et al.* 1999; Borgatti *et al.* 2005). It represents a surface of 1.6 km^2 of thick flysch and

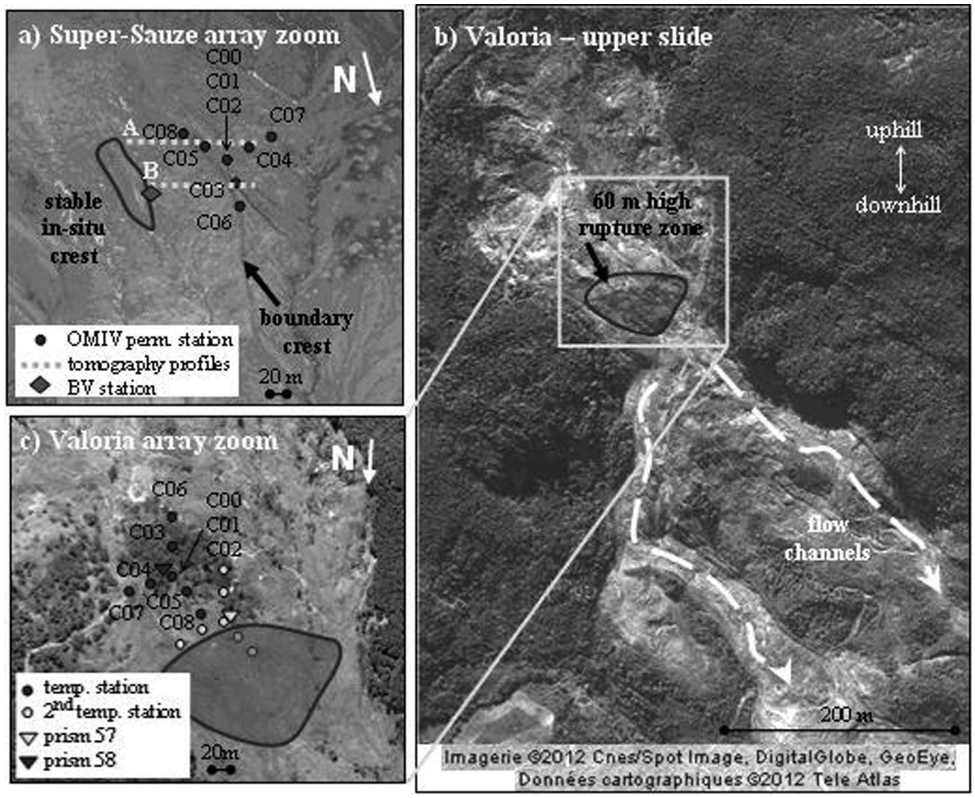

Figure 2. Presentation of the seismic arrays: (a) zoom on the seismic array at Super-Sauze, (b) Valoria upper part and (c) zoom on the array. For each picture, uphill is on the upper part of the figure and downhill on the lower part. The 3C sensor (channels C00, C01 and C02) is located at the centre of the tripartite array. Some geomorphological details (scarp, crest) are illustrated on the pictures. For Super-Sauze landslide, piezometric and rainfall parameters are measured at the BV station (a).

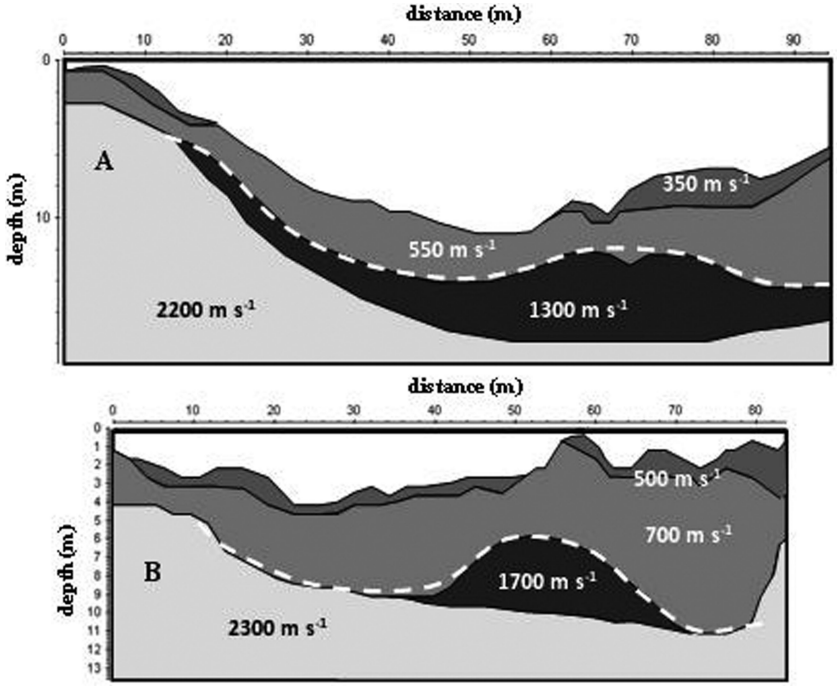

Figure 3. *P*-wave velocity profiles situated on the upper (a) and the lower (b) part of the seismic array at Super-Sauze, as indicated in Fig. 2a. The white-dashed line indicates the main discontinuity that have been imaged by the previous tomography analysis (Grandjean *et al.* 2006; Méric *et al.* 2007; Travelletti & Malet 2012).

clay–shale moving between 520 and 1413 m of elevation, with a 3.5 km length and a width varying from 100 to 500 m. The landslide is characterized by a succession of small hills and valleys, associated to accumulation and draining zones, and is actually the union of two previous landslides at the elevation 1150 m (Figs 2b and c). For this reason, the Valoria landslide is defined with two rupture zones, two accumulation zones and one unique evacuation canal (Ronchetti 2008). Most reactivations occurred during the snowmelt periods, in April and May. Other reactivations occurred in the autumn but were caused by rainy summer periods (amounts > 250 mm) and important rainfalls in the following months (amounts > 400 mm; Ronchetti 2008). Displacements have been measured with photogrammetry and airborne laser scanner (Corsini *et al.* 2009a). Since 2008, an integrated Total Station—GPS monitoring system has been used to survey slope movements that have reached maximum rates of metres per day (Bertacchini *et al.* 2009). In 2006, displacement rates up to 0.50 m d^{-1} have been observed in the upper part (Ronchetti *et al.* 2007). Seismic tomography of the internal structure was obtained by passive seismic acquisition (Cusano *et al.* 2006) and refraction seismic and drilling (Baldi *et al.* 2009). These studies indicated a first 15-30-m-thick layer characterized by V_P varying from 700 to 1500 m s^{-1} sliding on a stable bedrock characterized by V_P = 2500 m s^{-1}. Slip surfaces have not been detected with these acquisitions.

3 METHODS

3.1 Acquisition systems

At the Super-Sauze landslide, the seismic array has been installed for a permanent monitoring since 2009 October. The aim of this installation is to monitor the seasonal changes in microseismic activity according to the varying displacement rates of the landslides, and to characterize the possible influence of regional earthquakes. At the Valoria landslide, the seismic array was installed in 2009 November for a short monitoring period in order to compare the seismic signals detected at Valoria with those detected at Super-Sauze.

The passive seismic acquisition systems consist in seismic arrays with a 20 and a 40 m radius as illustrated in Figs 2(a) and (c). This type of array configuration has been introduced by Joswig (2008) as 'nanoseismic monitoring' in order to detect and locate small seismic signals. For both landslides, one three-component (3C) sensor is situated at the centre of a tripartite-shaped array and six vertical sensors are situated at approximately 20 and 40 m in the three directions of the array. As pointed out by Joswig (2008), this configuration allows a good correlation between channels. We used mostly vertical sensors because our location method uses only vertical sensors. Three-component sensors could be used to estimate the polarity of seismic waves, and thus the direction of the seismic source, if *P*- and *S*-waves are well separated, which is unfortunately not the case for seismic signals produced by muddy landslides. At both sites, the seismic arrays were located in the upper parts of the landslides characterized by the presence of fractures in the first 2 m of sediments.

At Super-Sauze, only one seismic array was installed in the upper part at the interface between the most active zone of the landslide (in terms of surface displacement) and a stable zone; at Valoria, two seismic arrays were installed in the upper part of the landslide (Fig. 2c). At both sites, the datalogger is a Képhren Agécodagis. The sensors are velocimeters with different characteristics for each landslide (Table 2). Data sampling rate has been set to 400 Hz, as the best compromise between signal resolution, data storage and data transmission. For both sites, the ground motion is recorded with a flat frequency response in the frequency range [2–80] Hz simultaneously on all channels of each array.

Table 2. Sensors characteristics.

Study case	Super-Sauze	Valoria
Data Logger	Képhren Agéodagis	Képhren Agéodagis
Sensors (velocimeters)	Noemax Agéodagis	2 Hz CJDZ
[Associated bandpass]	[0.1–80] Hz	[2–80] Hz
Sensitivity	1500 V m^{-1} s^{-1}	1920 V m^{-1} s^{-1}
Sampling rate	400 Hz	400 Hz

At the Super-Sauze landslide, additional observations consisted in surface displacements monitored ca. 60 m downhill of the seismic array through permanent GPS and one extensometer (Malet *et al.* 2002). The changes in groundwater table level are monitored with a Diver water height sensor installed in a 4.5 m deep piezometer called BV, and located at the vicinity of the GPS receiver and extensometer. The rain amounts are monitored with an automatic rain gauge located outside of the landslide, at a distance of 500 m (Malet 2003; Fig. 2a). At Valoria, two topographic prisms were installed close to the two seismic arrays to monitor the surface displacements (Fig. 2c). The displacements of the benchmarks were monitored by an automated TPS Leica Total Station (Bertacchini *et al.* 2009; Corsini *et al.* 2009b). The rain amounts are recorded at the Fontanaluccia raingauge station (municipality of Frassinoro).

At Valoria, because of an important acceleration of the landslide, the two seismic arrays have been damaged. The sensors were displaced for several metres and were deteriorated so that we recovered only partially the observations. We could only use these records as spatial and temporal evidences of the acceleration (discussed further).

3.2 Acquisition periods

The surface displacements observed at the Super-Sauze and Valoria landslides are variable along the seasons and can reach up to tens of centimetres per day in the spring period. Periods characterized by displacement of up to a few metres per day may be measured in extreme cases especially in the upper parts of the slides (Malet *et al.* 2002; Ronchetti *et al.* 2007). Both landslides are also characterized by the presence of compression and extension zones revealed by specific surface geomorphological features such as lobes, extension ridges and fissures (Travelletti *et al.* 2011).

In order to analyse the microseimicity pattern associated to different types of kinematic regime, three different acquisition periods were selected. Seismic signals respectively observed for periods of small displacements (<0.01 m d^{-1}), of moderate displacements (<0.10 m d^{-1}) and of very large displacements (>0.10 m d^{-1}) are analysed, respectively for a period of 2 weeks in 2009 October at Super-Sauze, for a period of 4 weeks in 2010 May at Super-Sauze and for a period of 10 d in 2009 November at Valoria.

3.3 Seismic signal detection

Because of an important amount of events, the semi-automatic detection method of Helmstetter & Garambois (2010) is used. This method has proved to be a useful tool to detect several thousands of seismic events within rock slopes. It is based on the spectrogram of the signal, averaged over all vertical sensors of the array. Then, the

Table 3. Comparison between the reliability of the manual and the semi-automatic picking techniques.

Acquisition period Studied landslide	2009 October (2 weeks) Super-Sauze	2009 November (1 week) Valoria	2010 May (4 weeks) Super-Sauze
Automatically picked candidate events	2097	12287	2082
After manual control	755	1615	1529
Manual picked events	710	Not tested	874

spectrum of the signal is normalized for each time window (sliding window of 128 samples) by the spectrum of the noise. The amplitude of the normalized spectrogram is summed in the frequency range [1–50] Hz. One seismic signal is detected when this function exceeds a threshold that has been fixed at 2, which means that the amplitude of the seismic signal spectrum must be at least twice higher than the noise to define a seismic signal. Seismic signals are chronologically listed in a catalogue, which contains the dominant frequency, the maximum amplitude of the seismogram (computed in the frequency range [1–50] Hz and averaged over all vertical channels of the array) and the time duration for each event. The duration corresponds to the period when the amplitude of the seismic signal is higher than the noise. All the seismograms and spectrograms listed in the catalogue are then analysed visually. Some signals were identified as likely corresponding to anthropogenic activities (ski lifts, helicopters, electrical devices, fieldworkers) or other sources of noise (storm, water runoff, wind), based on the frequency content of the signals and their temporal distribution, and by comparison with signals detected on other landslides (Helmstetter & Garambois 2010; Gomberg *et al.* 2011).

Semi-automatic detection was applied for the three acquisition periods. The number of seismic signals that were classified as noise is variable with the acquisition periods (Table 3), probably due to changes of anthropogenic activities and meteorological conditions.

To define the robustness of the semi-automatic detection method, the SonoView package (Joswig 2008; Sick *et al.* 2012), was used to detect visually the seismic signals and propose a reference (e.g. manual) catalogue. Spectrograms are calculated for each vertical channel with a sliding window of 256 samples with an overlap of 50 per cent, so that each pixel on the time axis of the spectrograms corresponds to ∼[128 samples/400 Hz] seconds. A global spectrogram, also called 'super-sonogram', is obtained from the combination of the spectrograms of all vertical channels of the array, pixel by pixel. Though this procedure, each pixel of the super-sonogram is made up with seven subpixels (Sick *et al.* 2012), extracted from the spectrograms of all vertical channels. The super-sonogram is then normalized by the noise spectrum. This enables a continuous clearer and more condense view of the variations for all vertical channels together. All seismic signals have to be considered manually individually, by observing the amplitude and frequency variations. HypoLine software, which is included in the SonoView package, enables us to determine further characteristics of the seismic sources such as the location in a layered velocity model (see section 3.4.3).

The semi-automatic and manual catalogues were compared for the 2009 October and the 2010 May records. After manual control of the candidate seismic signals picked by the semi-automatic method, up to over 50 per cent more seismic signals were detected (Table 3). Seismic wave arrivals are hard to identify because of the attenuation and the fractured nature of the material and the complex structure of the slope. For this reason, the semi-automatic detection method proposed by Helmstetter & Garambois (2010) can be considered as an efficient tool to detect most of the seismic signals, in spite of the high attenuation of the clay materials. However, it is necessary to control visually the detected seismic signals.

3.4 Seismic signal location

3.4.1 Beam-forming method

A beam-forming method has been applied to automatically locate all seismic events. This method is based on the beam-forming method developed by Lacroix & Helmstetter (2011) and inspired by Almendros *et al.* (1999) and Roux *et al.* (2008). It has been proposed for locating seismic events when the first arrival is difficult to pick precisely. In this method, the position of the source and the seismic wave velocity are inverted by maximizing the temporal correlation between the traces at all pairs of vertical channels, after shifting each trace by the traveltime (Lacroix & Helmstetter 2011). In our case, both landslides are characterized by a complex geometry (several layers, heterogeneities) and the tomography results confirmed a large variability of seismic wave velocities. These heterogeneous structures strongly disperse and attenuate the high frequencies of the seismic waves and make it difficult to distinguish the first arrivals of *P*, *S* or surface waves (Helmstetter & Garambois 2010). For these reasons, the beam-forming method is a good alternative way to locate emergent seismic events. We use a time window of about one second around the starting time of the event and filter the seismic signal in the frequency range [2–50] Hz. The inversion starts with a grid search on both position and velocity. In space, we use a grid covering the whole landslide (about 600 m × 300 m) with a step of 10 m. For the velocity V, we impose that V is, respectively, in the range between 400 and 2500 m s^{-1} and 200 and 2700 m s^{-1} for Super-Sauze and Valoria, with a step of 300 m s^{-1}. For each position and velocity, we compute the average intertrace correlation C after shifting traces in time by the traveltime. Then we select the best position and velocity, corresponding to the largest C value, as the starting point for a simplex optimization. The depth of seismic events cannot be reliably estimated in the case of heterogeneous materials and when the source is located outside of the seismic array (Lacroix & Helmstetter 2011). For these reasons, the source is constrained to lie at the surface of the landslide, although some of the seismic events are located within the mass volume or at the boundary with the stable bedrock (Amitrano *et al.* 2007). The surface is defined by a Digital Elevation Models with a spatial resolution of 2 m at Valoria (Sterzai *et al.* 2010) and 5 m at Super-Sauze (Travelletti & Malet 2012). Because the source depth is fixed at zero, the measured velocity V corresponds to an apparent velocity. Therefore, deep sources are characterized by a higher V compared with superficial events. The velocity parameter is thus useful for distinguishing external events (earthquakes) from local ones events triggered by the dynamics of the landslides. When using a single seismic array, the beam-forming method can only reliably estimate the direction of the source, but the distance between the source and the array is generally ill-constrained, as soon as this distance is

larger than the aperture of the array. In order to locate precisely the seismic sources, we would need to install several arrays around the active area, as done for example by Lacroix & Helmstetter (2011) for the Séchilienne rockslide.

3.4.2 Time correction through shot tests

Shot tests using an air-gun source were performed at Super-Sauze in 2010 July at 19 locations around the seismic array. The aim was to determine the reliability of the location and to estimate the static time corrections to account for variations of seismic wave velocity within the seismic array. Strong fluctuations of velocities are expected below the sensors of the arrays because of the variability of the characteristics of the material (e.g. sensors installed on soft water saturated, material and other sensors installed on more compact and drier material above the stable crests; Fig. 2a). The first *P*-wave arrival was picked manually for the 19 shots. We then computed the theoretical traveltimes between each source and each shot. We used a uniform seismic wave velocity, which was inverted for each shot by minimizing the residuals between picked times and theoretical arrival times. Finally, the static correction was estimated for each sensor by the average difference between picked and calculated arrival times following the method of Lacroix & Helmstetter (2011). One sensor (C03) was out of order during the shot tests, and thus the time correction was set to zero. Negative time corrections indicate that the picked times are generally earlier than the theoretical arrival times. This should correspond to zones with a velocity larger than the average seismic wave velocity. Surprisingly, we found negative time corrections for the sensors located in the most active part of the landslide (to the east) where we expected lower seismic wave velocities.

The static time correction was introduced in the location method by shifting each trace by its time correction as the first step of the location method. We tested the beam-forming location method, with and without correction. The calculated source position was sometimes situated up to 160 m away from the real source location, but this is not surprising since the beam-forming method cannot estimate reliably the distance for sources located outside of the network. For some cases, the direction of the source was also very different from the true direction, sometimes even on the opposite direction (Fig. 4). The location error is slightly smaller when using the static corrections: the average location error is 66 m without correction and 42 m with time correction. The direction of the source is also more accurate with corrections: the average azimuthal error is 46° without correction and 40° with correction. Finally, the intertrace correlation C is also slightly larger when using time corrections. Fig. 4 indicates that the location accuracy is generally better for shots with a larger intertrace correlation C. When C is larger than 0.48, the maximum azimuthal error is around 33° and the maximum horizontal error is about 40 m. These values should be kept in mind to evaluate the reliability of further event locations and to select only reliable events to map the microseismic activity.

Although the location accuracy of shots is quite bad, the location is probably more accurate for natural seismic signals. Indeed, some shots had a small signal-to-noise ratio and a high-dominant frequency. In comparison, many natural seismic signals have a lower dominant frequency and larger amplitudes, therefore a larger intertrace correlation and likely more accurate locations.

3.4.3 Manual location method

All shots were also located with HypoLine using manually picked *P*-waves arrivals, in order to compare the results of the automatic and the manual location methods. HypoLine (Joswig 2008) identifies the contribution of each single phase by displaying the 'hypoline' constraining curves. These hyperboles are obtained from one similar arrival picked at two sensors, or very rarely in our case, circles obtained if both *P*- and *S*-wave arrivals can be picked at one channel. The best solution is then characterized by the highest concentration of hypolines. For the HypoLine location, we used, at Super-Sauze, a seismic wave velocity model with two horizontal layers: a first 10-m thick layer with $V_P = 800\,\mathrm{m\,s^{-1}}$, over a half-space bedrock characterized by $V_p = 2300\,\mathrm{m\,s^{-1}}$. These values were derived from the tomography profiles (Fig. 3) and V_P/V_S ratio was comprised between 1.95 and 2.36. According to the shot tests, the manual method provides more accurate locations than the automatic one. However, we were influenced by the knowledge of the true positions of the shots when picking the shots manually and we obtained the final results only after adjusting the picked times several times. For this reason, we consider that the automatic location of Lacroix & Helmstetter (2011) can be trustfully applied to locate the detected

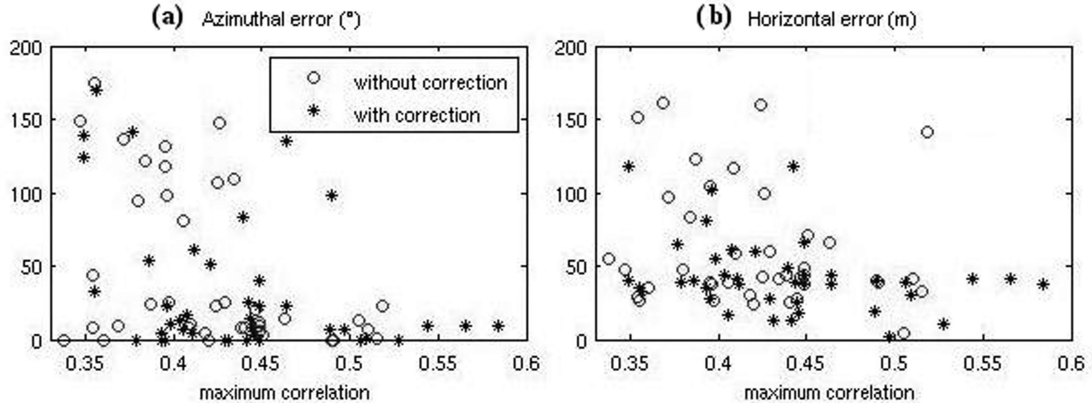

Figure 4. Azimuthal error (a) and horizontal error (b) versus the maximum intertrace correlation value for each air-gun shot test effectuated at Super-Sauze landslide: without (circles) and with (stars) static time correction. Without correction, the averaged azimuthal error is 44° and the averaged horizontal error is 61 m, whereas with correction, the averaged azimuthal error decreases to 34° and the averaged horizontal error decreases to 43 m. Without or with static time correction, shots located with a maximum intertrace correlation higher or equal to 0.48, tend to have a maximum azimuthal error of ca. 33°, from the centre of the array and a maximum horizontal error of around 40 m (except for one point).

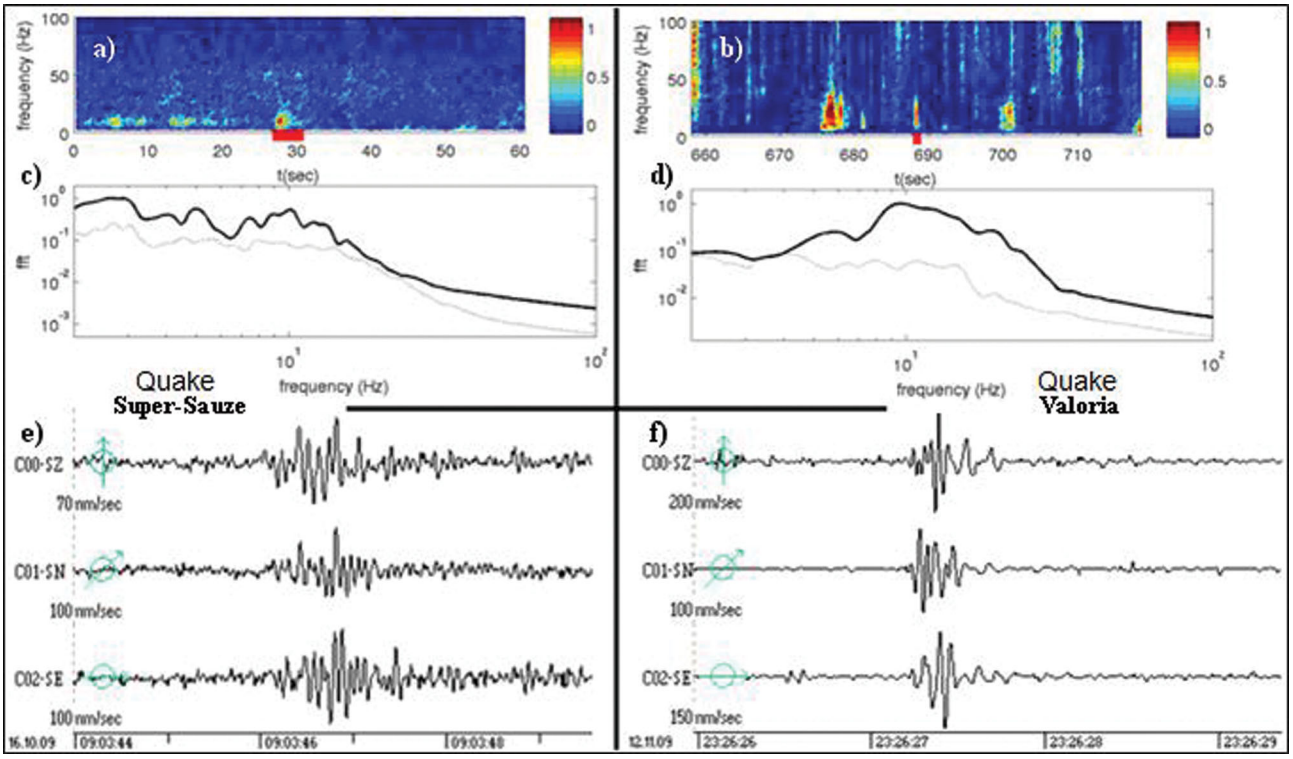

Figure 5. Example of seismic signals associated to quakes and detected at Super-Sauze (left) and Valoria (right): (a) and (c) spectrogram (averaged over all vertical sensors), (b) and (d) Fast Fourier Transform of the seismic signals (black line) and of the noise (grey line), (c) and (f) zooms of the seismograms of the 3C sensor (C00 is the vertical component, C01 is the north–south component and C02 is the east–west component). Time length of the seismograms corresponds to the red line on the spectrograms (a and b). Seismograms are [2–30 Hz] filtered.

natural seismic signals at Super-Sauze landslide, or at least to provide the azimuth of the sources. The beam-forming method has the advantage of saving a lot of time compared with the manual method. Also, it may be more efficient than the manual method for natural seismic signals, which are often emergent and difficult to pick.

As no shot test campaign was carried out at Valoria, we consider only the seismic signals located with a maximum intertrace correlation higher or equal to 0.48. This value cannot provide information about the location error threshold (as was defined at Super-Sauze) but it might limit too many incorrect source locations.

4 RESULTS

4.1 Classification of seismic signals

Following the approach of Walter & Joswig (2009) and Helmstetter & Garambois (2010), the seismic signals are classified in three groups named 'quakes', 'rockfalls/debris flows' and 'earthquakes'. The two first groups are associated to the dynamics of the landslide by itself, either at the surface or at depth; the last group corresponds to regional earthquakes not directly linked to the dynamics of the landslide. The classification associates quantitative (duration, apparent velocity, mean frequency) and qualitative criteria such as the wave phase identifications and the global spectrogram signature. Time duration, frequency content, apparent velocity and correlation between channels are the most significant discriminating parameters. For the landslide triggered seismic signals, the distinction between 'quakes' and 'rockfalls/debris flows' is rather difficult. It is done by comparing characteristics of events detected at Valoria and Super-Sauze with seismic events described in the literature by Walter & Joswig (2009) and Walter *et al.* (2011) for the Super-Sauze landslide, and by Helmstetter & Garambois (2010) and Lacroix & Helmstetter (2011) for the Séchilienne rockslide. Contrary to Walter & Joswig (2009), we only select seismic signals that can be identified visually on at least three sensors. In our cases, because of the high attenuation and the proximity between the sources and the sensors with respect to the wavelength, the different types of seismic waves are mixed together. Distinct *P*- and *S*-waves are only observed for earthquakes, which are located at least several kilometres away from the seismic array. Examples of all types of events detected either at the Super-Sauze or Valoria landslide, are illustrated in Figs 5–7. All seismograms are [2–30] Hz bandpass filtered, since it happens to be the dominant frequency range of seismic events.

4.1.1 Quakes

Seismic signals classified as 'quakes' have a duration of about one second and dominant frequencies around 10 Hz. The signal is generally emergent so that first arrivals are difficult to pick. We cannot distinguish successive *P*- and *S*-waves for these signals. This is likely due to the low-frequency content of the signal and to the short distance between the source and the sensors, so that *P*- and *S*-waves are mixed together. The envelope of the signal shows generally only one peak and has a symmetrical shape, with a progressive increase and decrease in amplitude with time. But a few seismic signals have higher frequency content and/or are composed of several subevents. In this case, the distinction between 'quakes' and 'rockfalls' is difficult and rather arbitrary.

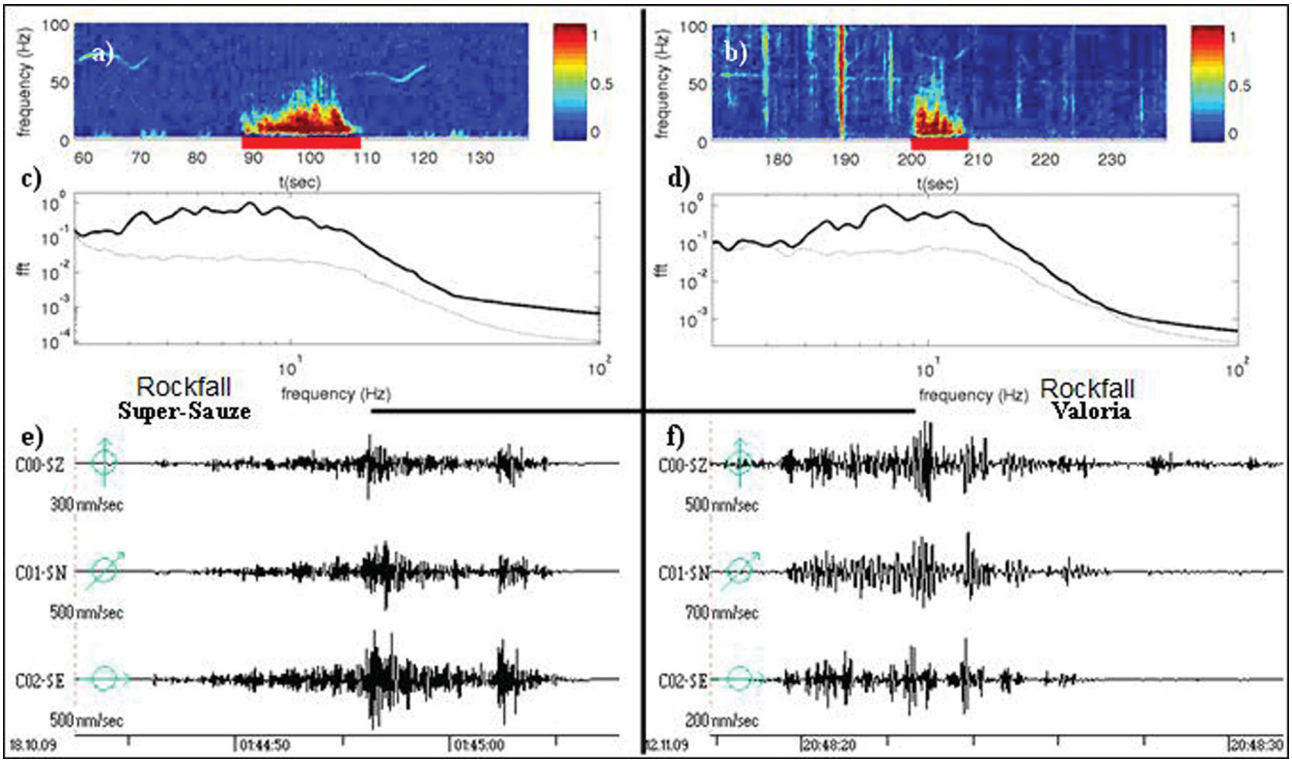

Figure 6. Example of seismic signals classified as rockfalls and detected at Super-Sauze (left) and Valoria (right). Same caption as in Fig. 5.

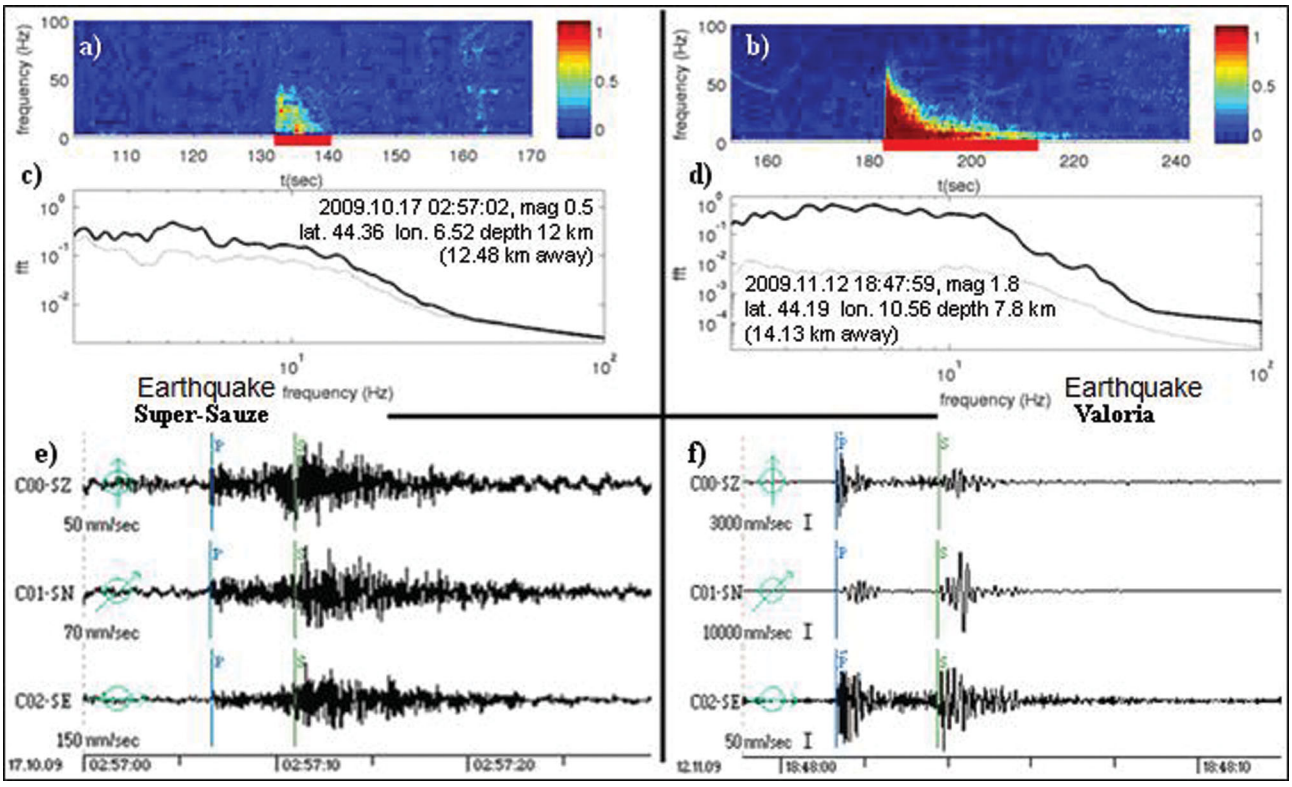

Figure 7. Example of seismic signals associated to earthquakes detected at Super-Sauze (left) and Valoria (right), and respectively by the SISMALP (Thouvenot *et al.* 1990) and the INGV seismic networks. Same caption as in Fig. 5, with date, magnitude, location and distance between the source and the landslide. The blue and green lines illustrate the *P*- and *S*-seismic wave arrivals.

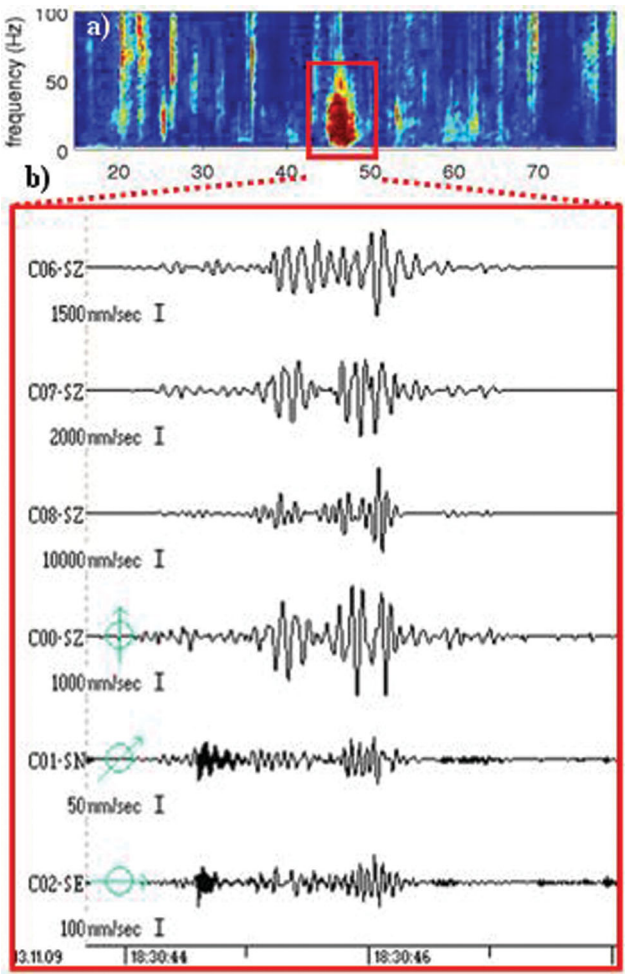

Figure 8. Example of a fissure event recorded during Valoria landslide acceleration: (a) averaged spectrogram and (b) seismograms of the three external vertical sensors and each channel of the 3C central sensor. Note the different amplitude scales between the channels.

These events are similar (in terms of duration and frequency content) to the seismic events detected by Helmstetter & Garambois (2010) at the Séchilienne rockslide. These events were suggested to be produced by slip or fracture opening. Walter *et al.* (2011) detected seismic signals associated with fissure opening at Super-Sauze with characteristics similar to some of our events identified as quakes (Fig. 8). These events were located on a fissure that was monitored by extensometers (Walter *et al.* 2011). The induced seismic signals had significant variations of amplitude among all sensors due to the proximity between the source and the sensors.

4.1.2 Rockfalls/debris flows

Seismic signals associated to rockfalls or debris flows correspond to longer signals of up to several tens of seconds. These signals are often composed of many subevents with time delay between successive peaks of about one second. The frequency content is mainly in the range [2–30] Hz. These signals sometimes repeat themselves during several minutes. The main difference with seismic signals classified as 'quakes' is thus the signal duration. It is therefore difficult to distinguish one rockfall seismic signal from several successive quakes.

4.1.3 Earthquakes

Seismograms of earthquakes show two clear arrivals with a time delay varying from about one second up to several tens of seconds (Fig. 7). Also, the amplitudes are often different for the vertical and the horizontal channels. The first arrival is generally impulsive and has higher frequencies. The second arrival is followed by a coda with a progressive decrease in amplitude and dominant frequency. The frequency content is very variable. Longer seismic signals have lower frequency contents (around 2 Hz dominant frequency), while events lasting only a few seconds have energy above 100 Hz. The shape of the envelope is asymmetric, with a sharp rise followed by a slow decrease. These signals can be easily distinguished from local events (quakes or rockfalls) by their higher apparent velocity (larger than 1000 m s^{-1}) due to their deeper source. Moreover, many of these events are coincident with earthquakes listed in either the French SISMALP earthquake catalogue (Thouvenot *et al.* 1990) or the INGV Italian earthquake bulletin. The seismic signals that are not present in earthquake catalogues have generally a short duration and small amplitude; they are likely small regional earthquakes located a few (tens of) kilometres away from the landslides.

4.1.4 Characteristics of seismic signals for all types of events

If the dominant frequency is plotted as a function of seismic signal duration (Fig. 9), the three types of seismic signals seem to concentrate in three poles. The most discriminating parameter appears to be the event duration. Signal amplitude is not considered as a selection criterion since it does not systematically vary between each type of event. Indeed amplitude varies from tens to thousands of nm s^{-1} for signals of the same type (Fig. 10). The peak amplitude of all signals is estimated after [2–50] Hz bandpass filtering. For each acquisition period, the distribution of amplitudes for local events follows a power-law for amplitudes larger than 300 nm s^{-1} with an exponent *b* comprised between 1.1 and 1.9. These values are comparable to those obtained at Séchilienne (Helmstetter & Garambois 2010; Lacroix & Helmstetter 2011), but larger than what Walter *et al.* (2011) evaluated at Super-Sauze, specifically for what they named 'fissure events'. The *b* value for quakes is different at Super-Sauze landslide for 2009 October and 2010 May acquisitions. However, because of the small number of quakes with amplitude larger than 300 nm s^{-1}, this difference is not significant. The roll-off for small amplitudes is probably due to the fact that small events can be missed because of variations of the noise level.

4.2 Seismic signals location

We applied the location method of Lacroix & Helmstetter (2011) described in section 3.4 to locate the local seismic events classified as either 'quakes' or rockfalls.

4.2.1 Location of seismic events at Super-Sauze

At Super-Sauze, the beam-forming location method was applied both with and without static time correction to check the reliability of location. By adding time correction, the locations are more concentrated and less focused along the grid-search boundaries. However, for seismic events located outside of the seismic array, the beam-forming location method does not provide a reliable estimate of the distance between distant sources and the seismic array.

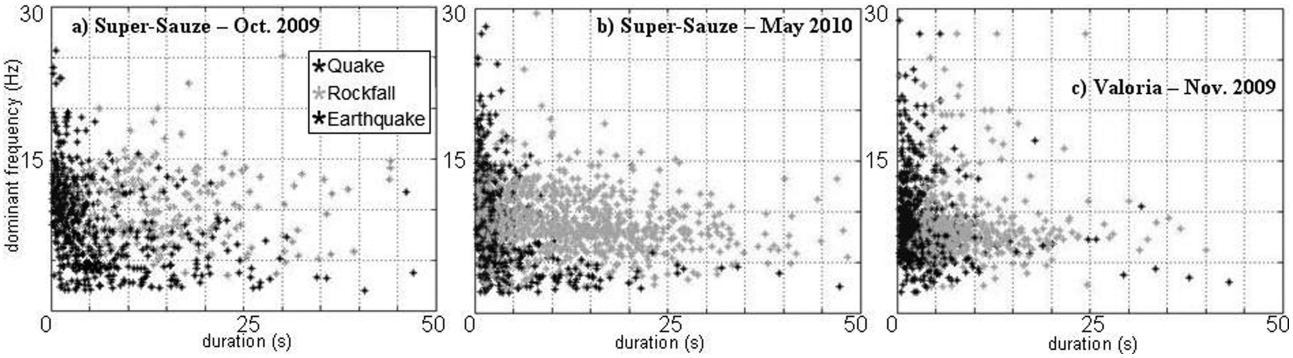

Figure 9. Dominant frequency versus time duration of the seismic signals detected during the three acquisition periods. Each type of seismic signals tends to concentrate around different regions of the plot.

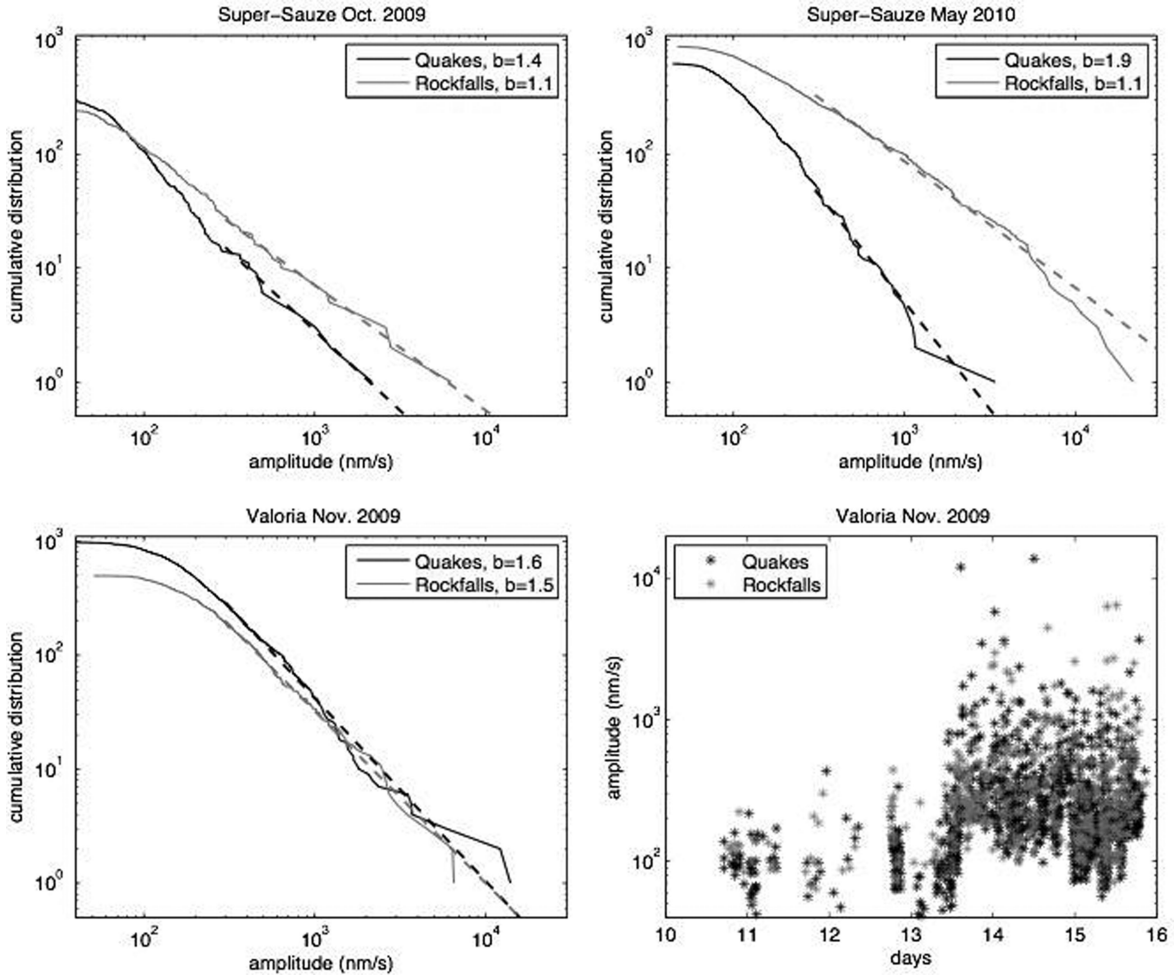

Figure 10. Cumulative distribution of seismic signals amplitude for local seismic events detected at Super-Sauze in (a) 2009 October and (b) 2010 May and (c) at Valoria. (d) Variations of the amplitudes of seismic signals detected during the acceleration at the Valoria landslide. Amplitudes range between 10^2 and 10^4 nm s^{-1}. Fits by a power-law distribution for amplitudes larger than 300 nm s^{-1} are shown by dashed lines, the power-law exponent b is given on each plot.

In this case, the method is only able to estimate the direction of the sources. Fig. 11 shows the distribution of azimuth for all seismic events located with an average intertrace correlation larger than 0.48, in reference to the shot tests. We can observe that, except for the quakes detected in 2009 October, most seismic signals are located with a direction coming from the southeast, corresponding to the upper part of the landslide. In Fig. 12, we present the seismic events located with an average intertrace correlation larger than 0.48 and inside the grid-search, excluding those located on the boundaries. By this way, about 60–70 per cent of local seismic events are located (Table 4) and cluster in different parts of the landslide. The spatial distribution of seismic events is approximately the same for both 2009 October and 2010 May acquisition periods. The main clusters are situated within the seismic array and in the upper part

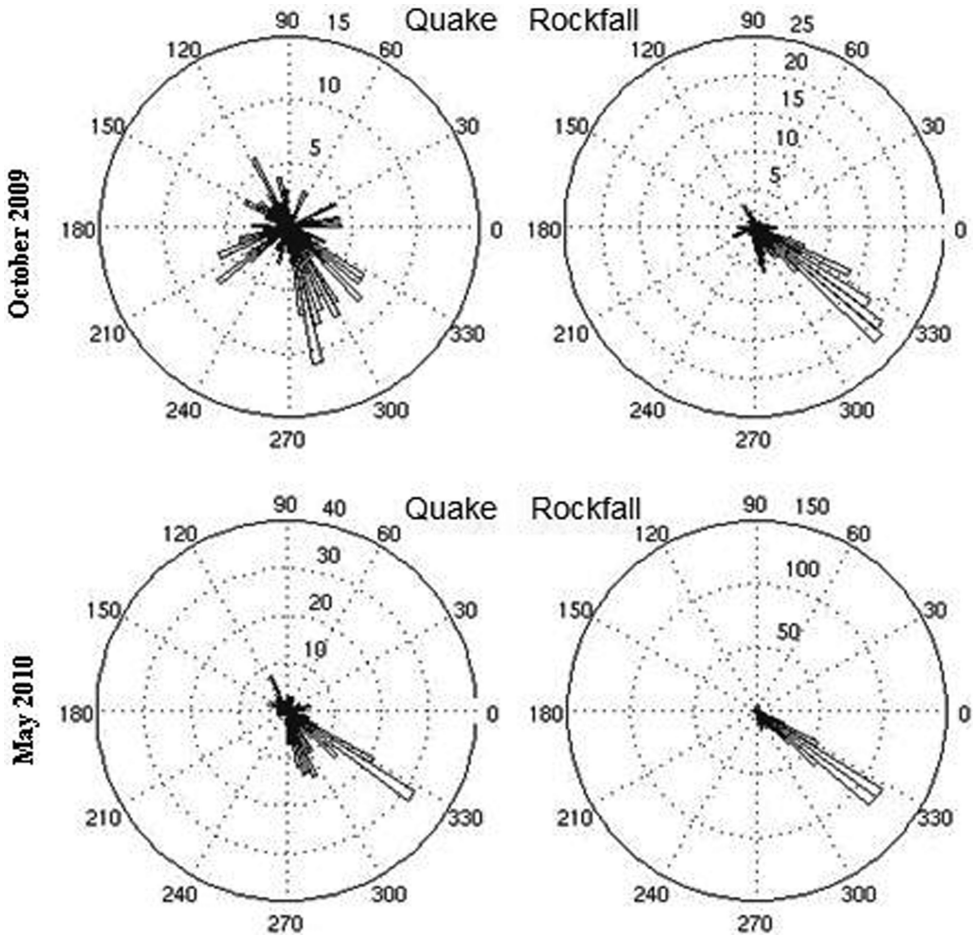

Figure 11. Azimuthal distribution of local seismic events located with an intertrace correlation higher than 0.48 and orientated from the centre of the seismic array, for 2009 October and 2010 May acquisition periods at Super-Sauze landslide.

of the landslide. The existence of clusters of seismic sources and the fact that most of them are located inside the landslide validates our location method.

4.2.2 Location of seismic events at Valoria landslide

A significant acceleration of the landslide occurred during the data acquisition and damaged the seismic arrays. Sensors were torn out and/or covered by clay materials and a 50-cm diameter stone hit the 3C sensor. The acquisition of the second seismic array (situated at the lower side) was interrupted on November 13 at approximately 19:21 (Table 5). The corresponding acquisition system and sensors of both arrays were recovered by the mud more than 30 m downhill from the array. Five of the seven sensors of the first seismic array were progressively set out of order, starting from the ones located downhill (Table 5). This suggests that the sliding first started downhill of the array and progressively developed towards the upper part of the array (Fig. 13). The damage to the instruments inhibited us from locating seismic events efficiently during the complete acquisition period. Nevertheless, data recorded by unaffected or recovered sensors show a lot of seismic events located for different time periods towards the grid-search boundaries as azimuthal indicators of the events (Figs 14 and 15). All seismic events located with an average intertrace correlation greater than 0.48 are selected.

An increase in the number of seismic events is first observed in the morning of November 13. They were mostly quakes located nearby the seismic array (Fig. 14a). Progressively, the sources propagated downhill with the emergence of rockfall events, but there was still activity in the upper part (Fig. 14b). On November 14, the landslide continued to be quite active in the upper and lower parts (Fig. 14c). The activity slowly started to decrease from November 15. Seismic sources are concentrated nearby the seismic array (Fig. 14d). The location of the seismic signals was interrupted on the evening of November 15 because there were only two vertical sensors still recording. It is important to note that we assumed that the sensors were installed at their initial positions for the analysis, which is probably not realistic.

5 DISCUSSION

5.1 Comparison of microseismic activity and landslide kinematics

5.1.1 Seismic signal: quakes

At Super-Sauze, the two clusters of 'quakes' coincide with the presence of the shearing zone between the unstable and the more stable parts of the landslide (e.g. defined by the two crests; Fig. 2b), where shearing and fissure opening/closing are likely to happen. At

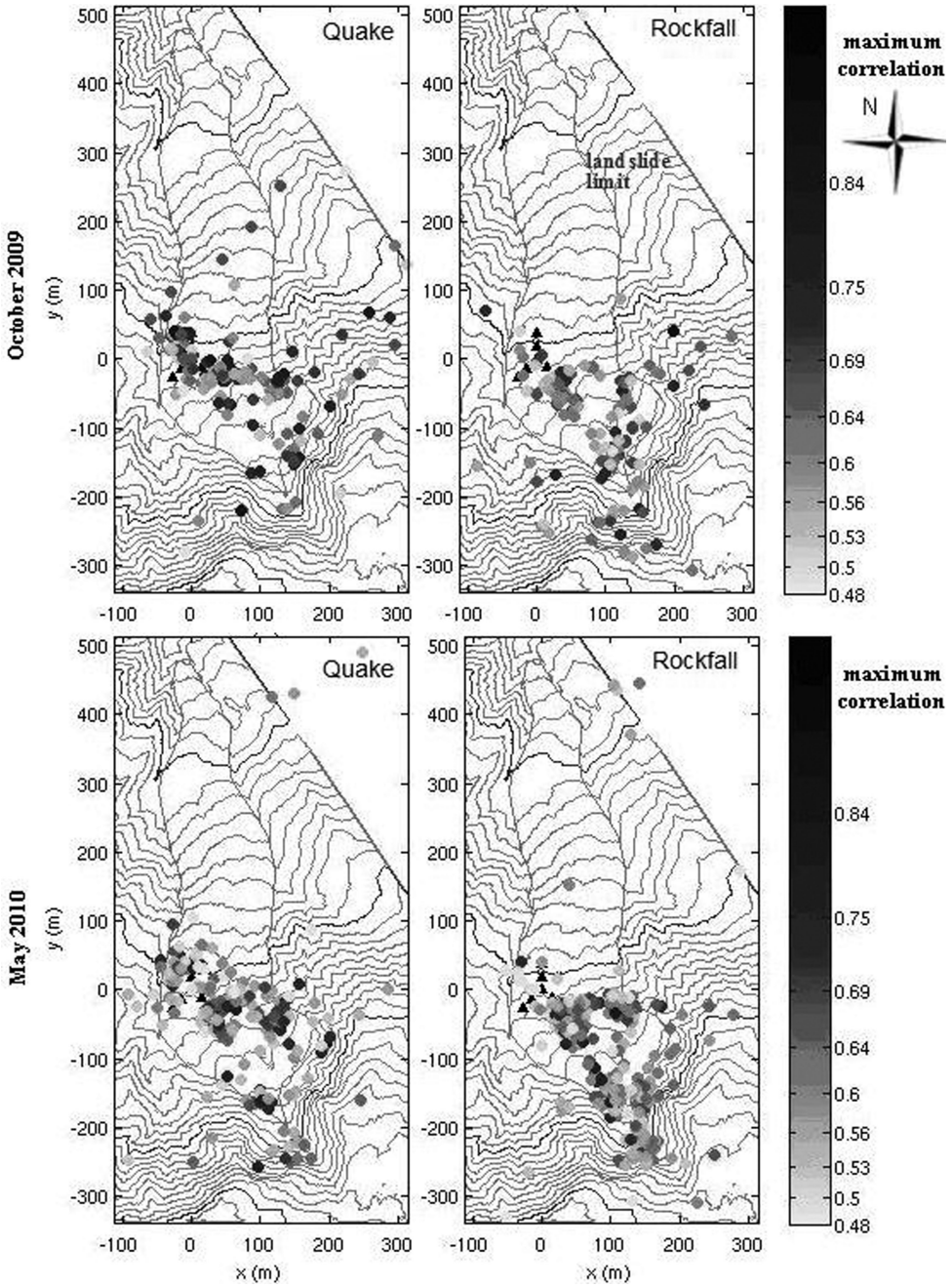

Figure 12. Location of seismic events in 2009 October and 2010 May at Super-Sauze landslide. Shade indicates the intertrace correlation (only events with $C > 0.48$ are selected). The black triangles are the sensors positions and the continuous grey contour represents the limits of the landslide.

Table 4. Number of seismic events detected at Super-Sauze and located on Fig. 12.

Acquisition period	2009 October (2 weeks)		2010 May (4 weeks)	
	Quakes	Rockfalls	Quakes	Rockfalls
Total number of seismic events	305	243	567	858
Number of seismic signals located inside the grid and with $C > 0.48$	206	177	311	576

Table 5. Times when seismic sensors of the first antenna were considered as out of order during seismic acquisition at the Valoria landslide. The time when the second seismic station stopped is indicated too.

Sensor number	C00	2nd station	C08	C05	C04	C03
Time when sensor is out of order	2009/11/13 00:00	2009/11/13 19:21	2009/11/13 20:45	2009/11/15 02:10	2009/11/15 16:00	2009/11/15 19:00

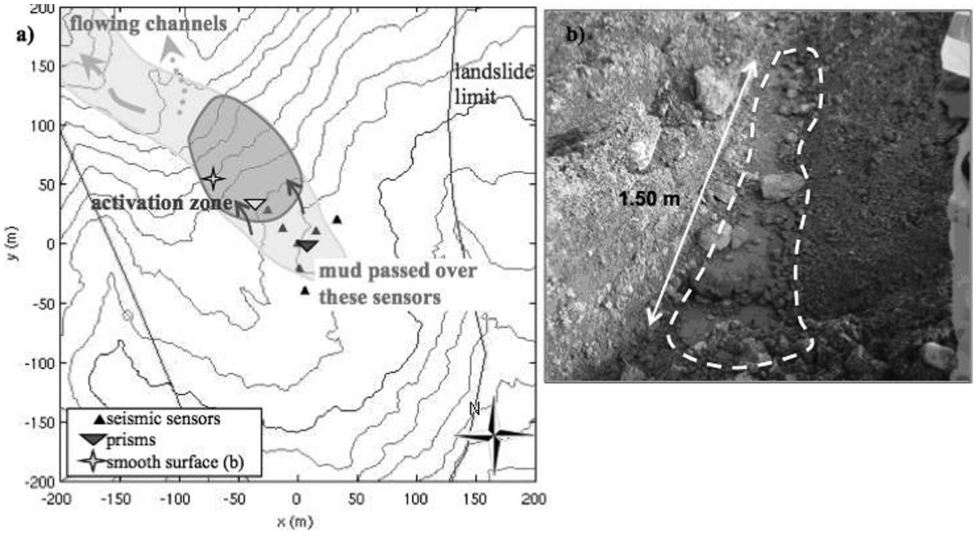

Figure 13. Schematic interpretation of the main acceleration and failure event at the Valoria landslide, on November 13 with evidence of the main failure zone (grey-out area on a): (a) global illustration and (b) element of the sliding surface: the white-dashed surrounded surface shows a smooth surface that we identified after the collapse.

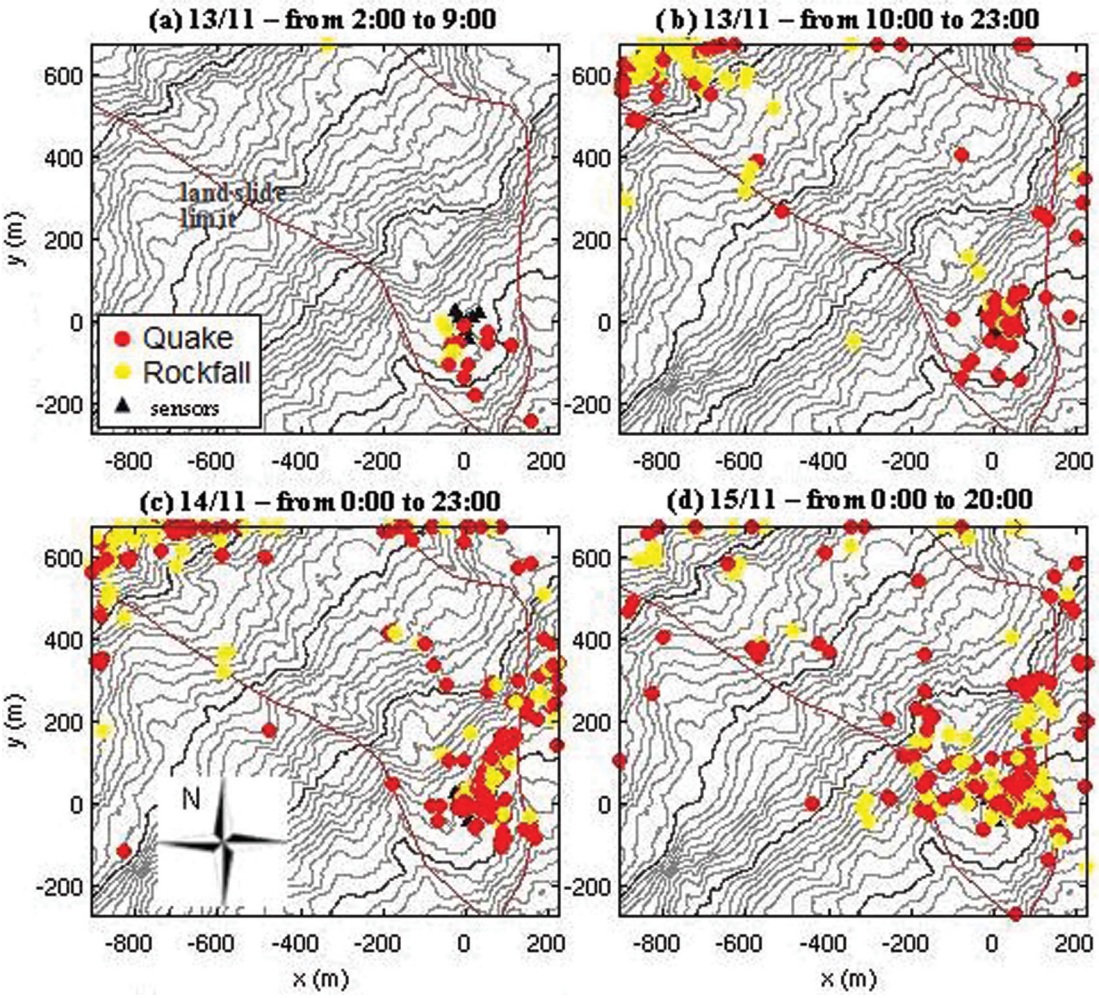

Figure 14. Progressive displacement of the source location for quakes and rockfalls during the acceleration phase at the Valoria landslide. The black triangles are the sensors positions and the continuous red contour represents the limits of the landslide.

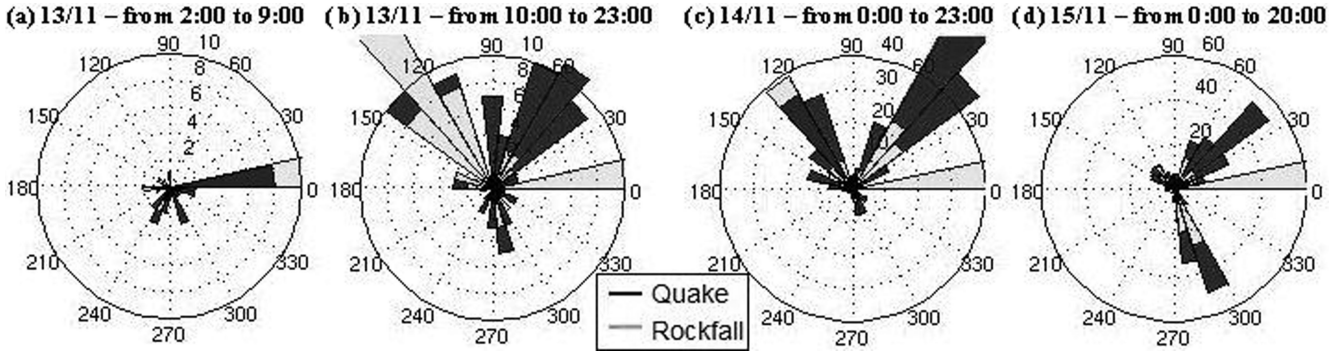

Figure 15. Progressive displacement of the azimuth of the source for quakes (dark grey) and rockfalls (light grey) during the acceleration phenomenon at the Valoria landslide on the azimuthal point of view. Note that the radius of the rose diagram might change during each phase.

Valoria, 'quakes' cluster essentially nearby the seismic array and the quantity of detected signals might vary with the slope phases (Fig. 14). After the main acceleration, we observed a ca. 5-m^2 sized fresh slip surface located below the seismic array (white dashed surface on Fig. 13b), which was not present at the start of the campaign. We assume that this discontinuity previously existed and is has been enlarged during the acceleration period.

We suggest that quakes are associated to friction processes, material deformation or fracture processes. The distinction between these phenomena is difficult unless the location of the seismic events in depth could be precisely estimated. The frequency content or the amplitude cannot be used as discriminating factors since these parameters are mainly controlled by the distance between the source and the seismic array.

5.1.2 Seismic signals: rockfalls and debris flows

At Super-Sauze landslide, rockfalls concentrate in the upper most active part of the landslide, at the level of the covered *in situ* central crest (Fig. 2b) or uphill at the main scarp. Seismic sources located near the main scarp can be identified as large rocks falling from the scarp, as suggested by Walter & Joswig (2009) and by field observations (visual observations and noise) during field campaigns. Seismic sources located within the *in situ* central crest are rather interpreted as brittle materials falling along the surface of the slide. The location accuracy does not allow us to distinguish trustfully seismic events located at the main scarp from events located within the landslide but far from the seismic array.

At the Valoria landslide, the first seismic signals associated to rockfalls or debris flows have been recorded a few hours after the beginning of the acceleration. We observed few seismic sources located on the upper part, in agreement with the absence of a scarp zone for this slide. Most rockfalls or debris flows are located downstream from the array, on the west side. Previous acceleration phases of the landslide generally initiated in the upper part of the slide (close to the seismic array) and then propagated downward and triggered the slide into the two main channels, on each part of the central ridge (Fig. 2c; Schädler 2010). The most active channel is the one situated on the northwest side of the central ridge (down right on Fig. 2c). We can thus interpret these events as due to the movement of clasts of different sizes. The first quakes that occurred during the early phase of the acceleration are thus coherent with the activation phase of the rupture preceding the sliding.

We suggest that the seismic signals classified as rockfalls are generated by the propagation of material on the surface, either as falls of blocks or debris from the upper scarp (at Super-Sauze landslide) or as small volumes debris flows at the landslide surface (at Valoria and Super-Sauze landslides). Arattano (1999) observed similar seismic signals with a longer duration during flow events of the Moscardo torrent in Italy. Helmstetter & Garambois (2010) also recorded seismic signals associated with rockfalls at Séchilienne rockslide. In this case, the classification as rockfalls was confirmed by a video record of some of these events. Compared with seismic signals at Super-Sauze landslide, rockfalls detected at Séchilienne had generally larger frequency content (up to 100 Hz), a longer duration, and a more irregular shape composed of many peaks due to successive rock impacts. The difference between Super-Sauze and Valoria landslides and Séchilienne rockslide seismic signals is likely due to the different materials involved and the rheology: micaschists at Séchilienne rockslide and clay–shales at Super-Sauze and Valoria landslides.

Alternatively, these seismic signals classified as rockfalls may be interpreted as 'tremors' generated by slow slip at the base of the slide or by fluid flow inside the slide (Travelletti & Malet 2012). Such long-duration and low-frequency events have been detected on volcanoes (Rouland *et al.* 2009) or on faults (Husker *et al.* 2010). Indeed, these tremors are usually interpreted as resulting from either fluid flow or slow slip on faults (e.g. Thomas *et al.* 2009). For landslides however, there has not been yet any observation of seismic signals associated with slow-slip events. A method for discriminating tremors from clasts slides or falls is to locate the source of the seismic signal in a sliding time window. At Séchilienne rockslide (Lacroix & Helmstetter 2011) or for snow avalanches (Lacroix *et al.* 2012), it was possible to follow the source propagating downwards. At Super-Sauze, we also detected a temporal variation of the source position during a few rockfall events. Fig. 16 shows the results obtained for a rockfall detected on 2010 May 31 at Super-Sauze. Because of the large uncertainty of locations, we imposed that the source is located along a north–south direction located at $x = -100$ m (approximately in the central part of the landslide). We divided the seismic signal into separate time windows of 2 s. For each time window, we fixed the velocity equal to 400 m s^{-1} (the value obtained for the first time window) and we only inverted for the north coordinate. We observed a propagation of the source northward at a velocity of 2.5 m s^{-1} (but this velocity depends on the absolute location of the source, e.g. on our choice of the east coordinate). This observation confirms, at least for this case, our classification of this seismic event as a rockfall or debris flow. Unfortunately, for most cases we could not observe a propagation of the source location. One explanation is that most rockfalls or debris

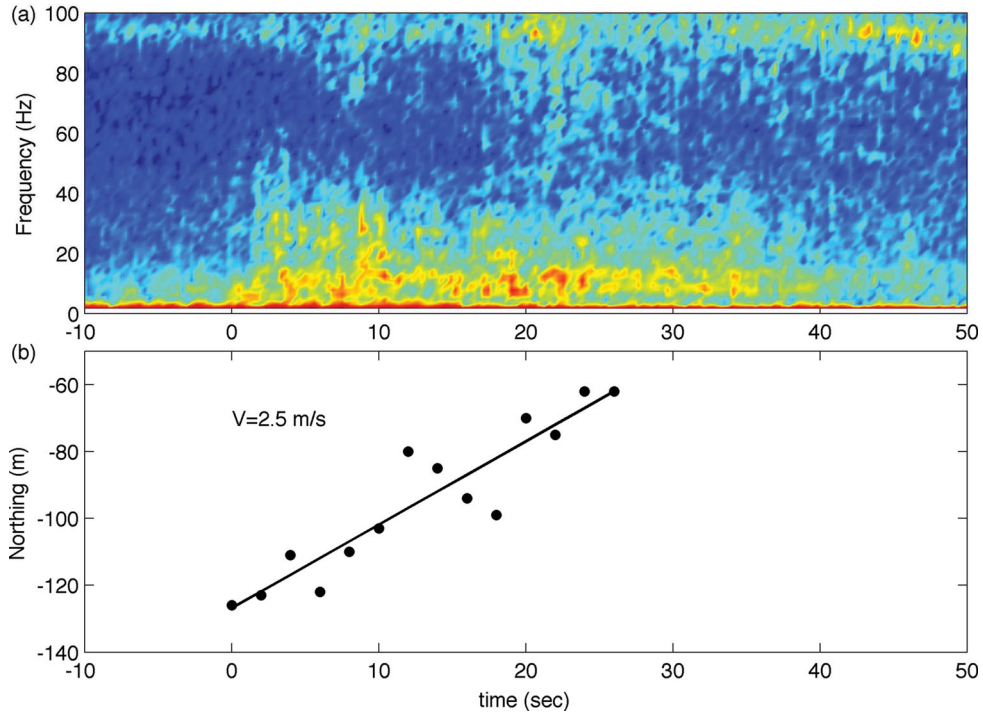

Figure 16. (a) Spectrogram of a rockfall signal recorded at Super-Sauze landslide the 2010 May 31 at 06:12 and (b) temporal variation of the source location during this rockfall event. V indicates the average propagation velocity of the rockfall. The source was imposed to be along a north–south line on the central part of the landslide (at $x = 100$ m), and only the y coordinate was inverted for each 2 s time window.

flows likely propagate toward the seismic array. In these cases, we cannot observe a source propagation because our location method is mostly sensitive to variations of the source azimuth but not to the variations of the distance.

5.1.3 Seismic activity and displacement

In Figs 17–19, we compare the temporal variation of the rate of seismic events with the evolution of displacement, rainfall and ground water level during each seismic acquisition period. At Super-Sauze, we used all seismic events with amplitude larger than 100 nm s^{-1}, while we used only events larger than 200 nm s^{-1} at Valoria to be less sensitive to temporal variations of the noise level. At Super-Sauze, we used the displacement measured by an extensometer located nearby the *in situ* crest (Fig. 2a), about 60 m downhill from the centre of the seismic array. At Valoria, we used the displacements calculated from the monitoring of two benchmarks installed nearby the seismic arrays (Fig. 2c).

At Super-Sauze in 2009 October, Fig. 17 indicates one main peak of seismic activity on October 22 and two peaks of displacement rates. The main peak of displacement rate on October 20 occurs just before the increase in seismic activity while the second smaller peak of velocity (October 24) is not followed by an increase of seismic activity.

At Super-Sauze in 2010 May, the peak of velocity observed on May 8 occurs 1 d before the maximum of seismic activity, whereas the other peak of seismic activity on May 7 is not associated with a peak of velocity (Fig. 18).

At Valoria in 2009 November, the acceleration started on November 13 at the same time as the increase in seismic activity (Fig. 19). We could measure the displacement acceleration until the benchmarks were lost in the evening of November 13. The microseismic activity also increases in the morning, and then stays at a constant rate in the afternoon (Fig. 20). An interpretation is that the acceleration was triggered by fracture or sliding events associated with the detected seismic signals. Once the failure was activated, the movement accelerated while the microseismicity remained constant at a high rate. During the following days, the rate of quake events remained higher than the rate of rockfalls or debris flows.

In summary, the relation between local seismic activity and slope displacement is nontrivial and not systematic. To test quantitatively the correlation between velocity and seismicity rate, we computed the linear correlation coefficient between these quantities (Table 6). The correlation is positive and significant at Valoria. At Super-Sauze in 2010 May, we also found a positive correlation between rate of seismic events and velocity, but this correlation is not significant at the 95 per cent confidence level. There is indeed a probability p of 11 per cent that such a correlation may be found by chance. At Super-Sauze in 2009 October, the velocity was smaller than for the other acquisition periods. For this case, we found no correlation between velocity and seismic rate. Note that the displacement is measured at only one or two points for each landslide, and may not be representative of the average landslide displacement. This could be a reason why there is no systematic correlation between seismic activity and displacements, since many detected seismic events are located far from the points where displacement is measured.

5.2 Correlation of seismic signals with triggering factors

The rainfall amount and, in the case of Super-Sauze, the changes in groundwater table were monitored during the seismic monitoring campaigns. We compared the variations of seismic activity with these external meteorological parameters and with earthquake occurrences. These records are detailed in the Figs 17–19.

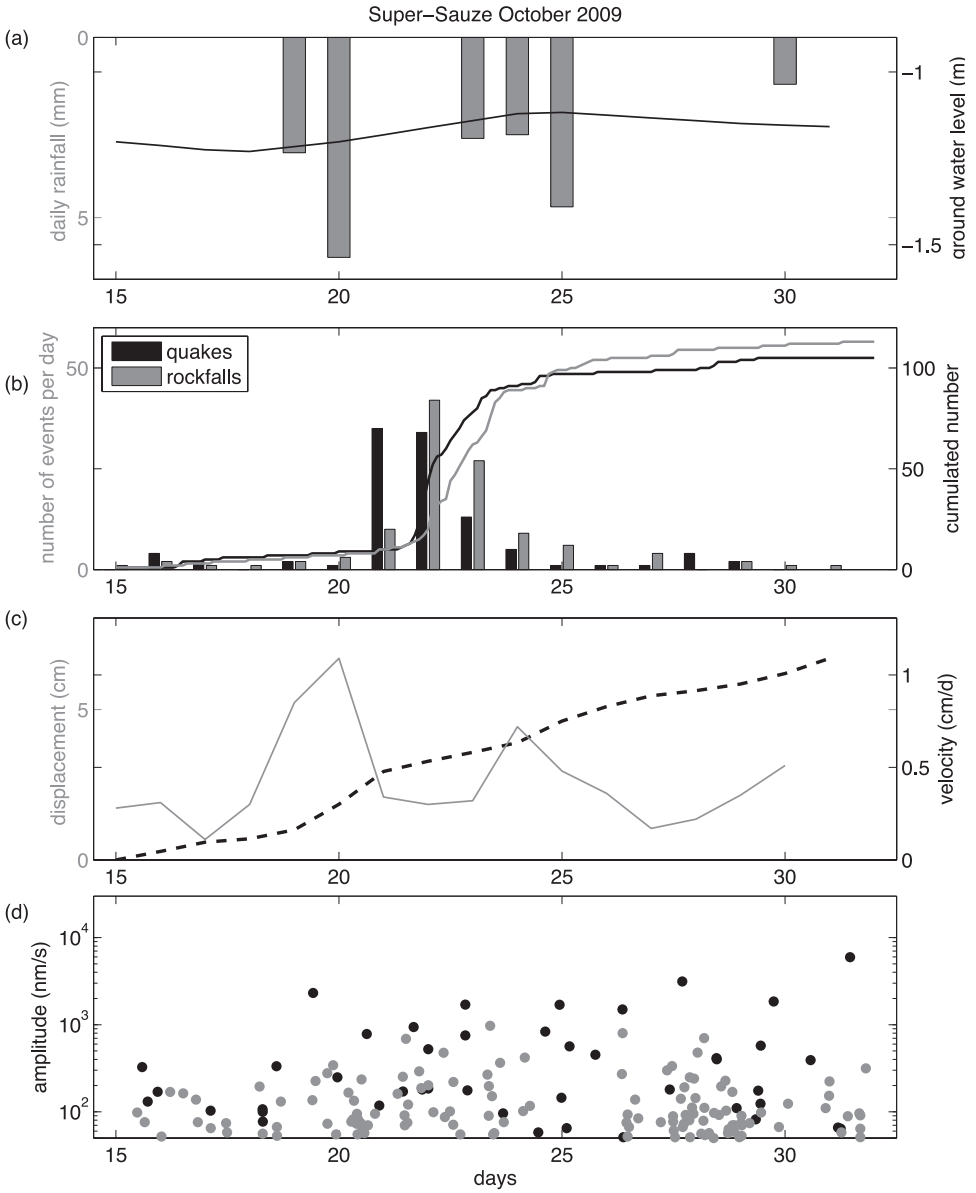

Figure 17. Temporal variations for Super-Sauze landslide in 2009 October of (a) rainfall and water table, (b) number of local seismic events, (c) daily cumulated displacement and velocity (derivative of the displacement) and (d) peak ground velocity of detected earthquakes. Black circles indicate earthquakes also detected by SISMALP or RENASS networks, while grey circles show events only detected at Super-Sauze.

5.2.1 Hydrometeorological triggering factors: rainfall and groundwater table

At Super-Sauze, rainfall occurred during the two acquisition periods and changes in the groundwater table level are observed (Figs 17 and 18). The spring period at Super-Sauze is characterized by snow melting. The saturation is higher, which probably influences the fragility of the material and may produce seismic events. At Super-Sauze landslide, the snowmelt periods ends ca. May 18 at proximity to the seismic array and later, on ca. May 26, uphill. A higher rate of rockfalls was recorded, essentially between May 5 and 10. We can interpret this increase by changes in the soil moisture at the near-surface caused by the infiltration of the melting water, and consequent small changes in the rheology of the clay. Indeed, Maquaire *et al.* (2003) have demonstrated from laboratory ring shear tests on samples that the cohesion of the Super-Sauze material may be drop down for small changes of water content. The water saturation is not necessarily the highest at the time of maximum snowmelt, because of delay in the transit of water within the material and of evapotranspiration fluxes. The rate of quakes also increased, possibly because the saturation level may induce fracture opening or closing.

At Valoria, important rainfall amounts were recorded during the 10 d preceding the installation of the seismic array (Fig. 18). The rain ceased on November 10, and the number of local seismic events started to increase on November 13. Previous landslide reactivations at Valoria were also generally triggered after 3–4 d of intense precipitation (Ronchetti 2008).

We calculated the linear correlation coefficient between the seismicity rate and the rainfall at Super-Sauze landslide to complete

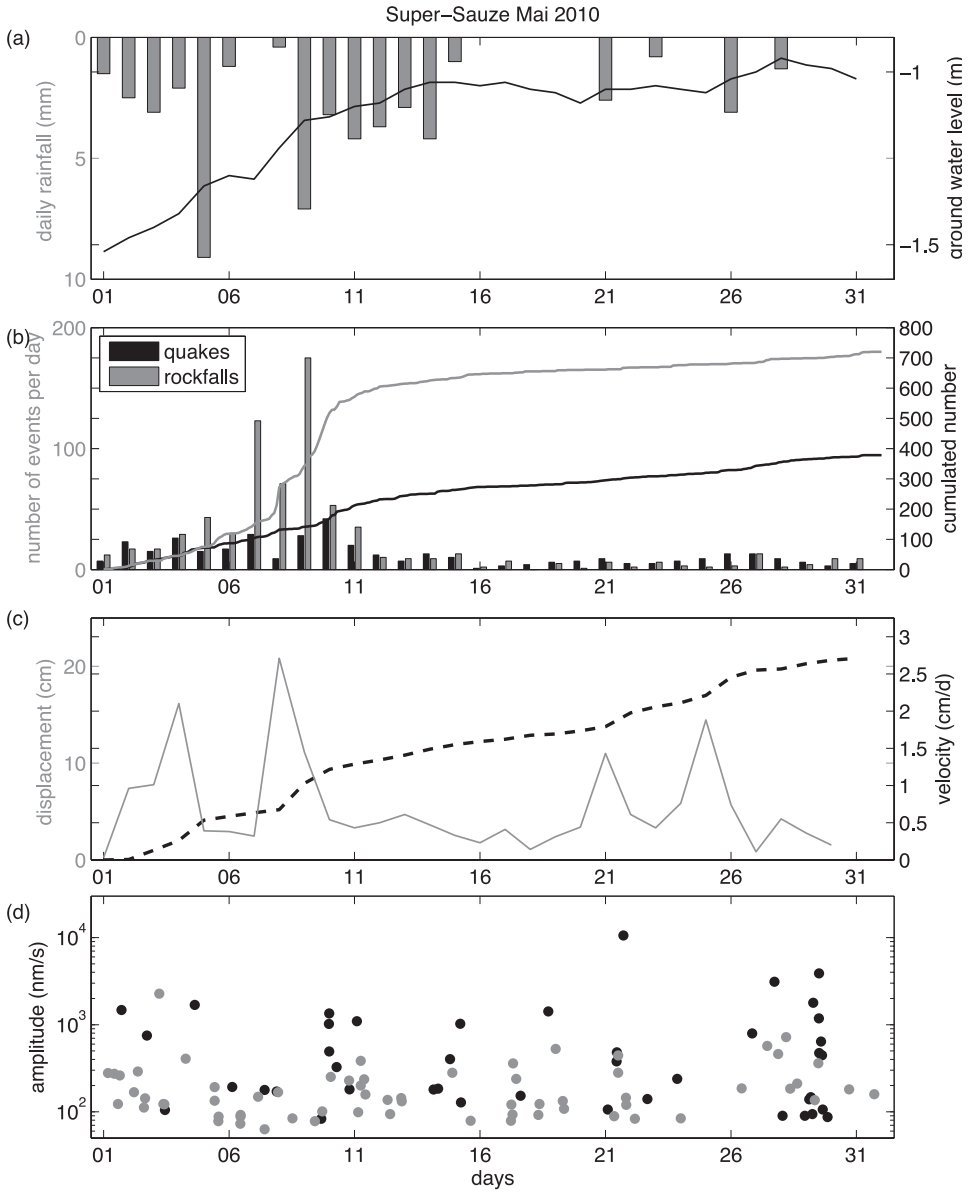

Figure 18. Temporal variations for Super-Sauze landslide in 2010 May of (a) rainfall and water table, (b) number of local seismic events, (c) daily cumulated displacement and velocity (derivative of the displacement) and (d) peak ground velocity of detected earthquakes. Black circles indicate earthquakes also detected by SISMALP or RENASS networks, while grey circles show events only detected at Super-Sauze.

this qualitative interpretation (Table 6). We found a positive correlation for 2010 May. For 2009 October however, the correlation is not significant at the 95 per cent confidence level, probably because the acquisition period is too short and the rainfall were not important during the acquisition period. The linear correlation is probably not a good mathematical tool to model the relation between rainfall and microseismic activity. Indeed, there is likely a time delay between rainfall and the triggering of rockfalls, debris flows or quakes. Therefore, a better way to analyse the influence of rainfall would be to compute the cross-correlation function between these two time-series, as done by Helmstetter & Garambois (2010) at Séchilienne rockslide. This method provides the response of the seismicity rate as a function of the time since the rainfall maximum. In our case however, the acquisition periods are not long enough to perform this analysis.

5.2.2 Geodynamic triggering factors: earthquakes

For the three acquisition periods, we detected many small earthquakes, especially during the 2009 October acquisition period at Super-Sauze. More than 200 earthquakes were identified in 15 d in 2009 October, against 107 in 31 d in 2010 May. For Valoria, we identified 18 earthquakes in 5 d. The largest recorded ground motion had a maximum velocity higher than 10^4 nm s^{-1}. The lower plot of Figs 17–19 illustrates the time of occurrence of earthquakes and their peak ground velocities. We do not see any triggering of local events after earthquakes. The sensibility of earthquake-triggered landslides has been highlighted since 1984 by Keefer (1984). In our cases, we did not reach the shaking intensity threshold to trigger any movement within the landslides (Keefer 1984, 2002).

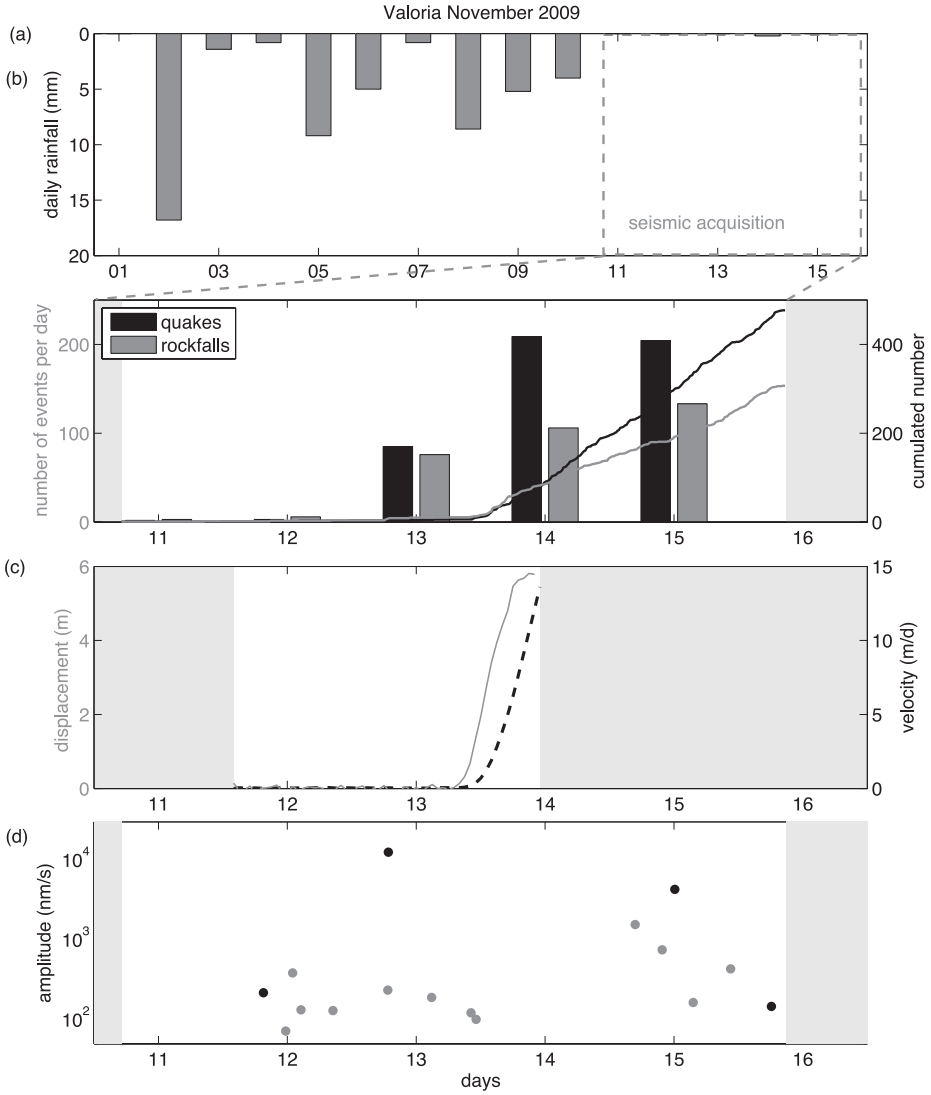

Figure 19. Temporal variations for the Valoria landslide in 2009 November of (a) rainfall, (b) number of local seismic events, (c) daily cumulated displacement and velocity (derivative of the displacement) and (d) peak ground velocity of detected earthquakes. Black circles indicate earthquakes also detected by the INGV, while grey circles show events only detected at Valoria. The framed part on (b) and (c) is zoomed on Fig. 20. Grey shaded areas indicate that data is not available.

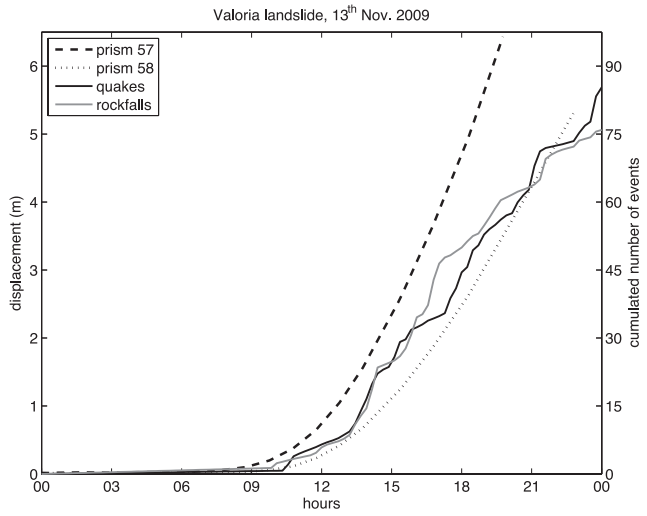

Figure 20. Zoom on the acceleration of November 13.

6 CONCLUSIONS

We applied seismic monitoring on two clay–shale landslides, Super-Sauze (France) and Valoria (Italy) in order to evaluate microseismic activity and to compare them with the landslide kinematics. We used a semi-automatic detection and location method (Helmstetter & Garambois 2010; Lacroix & Helmstetter 2011). Detection of seismic events is based on the spectrograms and seismograms analysis of the seismic signals recorded at several sensors of one seismic array. We checked the efficiency of this semi-automatic method by comparing with the 'nanoseismic monitoring' manual method proposed by Joswig (2008), which has already been successfully tested at Super-Sauze landslide (Walter *et al.* 2009). The semi-automatic detection and classification method (Helmstetter & Garambois 2010) proved to be an efficient way to detect weak seismic signals and moreover a time-saving solution. After manually controlling all the detected events, we identified three types of events, common to both Super-Sauze and Valoria landslides. Earthquakes were clearly identified and distinguished from local events

Table 6. Linear correlation coefficient (r) between the rate of seismic events, the velocity and the rainfall. The correlation is significant at the 95 per cent confidence level if $p < 0.05$. The p is the probability of getting a correlation as large as the observed value by random chance, when the true correlation is zero. The rates of displacement and of seismic events are estimated every day at Super-Sauze but every hour at Valoria.

Acquisition period	2009 October (Super-Sauze)		2012 May (Super-Sauze)		2009 November 11–13 (Valoria)	
Correlation between	r	p	r	p	r	p
Seismic events and velocity	−0.141	0.603	0.299	0.109	0.870	0.000
Seismic events and rainfall	−0.070	0.790	0.460	0.009	No rainfall	

based on the existence of distinct *P* and *S* waves, on their higher apparent velocity, and for some events, on their coincidence with events listed in regional earthquake catalogues. Local events were classified as either 'quakes' or 'rockfalls/debris flows' based on their signal duration and other characteristics, but the distinction between these two types of events is not always trivial. Local seismic events were located using the beam-forming method of Lacroix & Helmstetter (2011). This method was tested by comparing with the HypoLine manual location software (Joswig 2008) based on manual picking of first waves arrivals, and, in the case of Super-Sauze landslide, by performing shot tests. These shots enabled us to estimate a static time correction for each sensor. Local seismic events were concentrated in several clusters, essentially nearby the array on fractured and creeping zones for quakes and on scarp and unstable zones for events classified as rockfalls. At the Valoria landslide, only some of the events could be located due to the occurrence of a collapse and the progressive loss of several sensors. We observed a progressive evolution of the type and of the location of seismic events during the acceleration of the slide, which started near the seismic array and propagated downstream. The slide turned into a debris flow downward the western channel of the landslide, as observed during previous reactivations (Ronchetti 2008; Schädler 2010). In this way, we could associate quake events to internal friction or fissure opening/closing. Longer seismic signals, which were classified as 'rockfalls', are probably due to gravels or rocks propagation along the slopes or falling from the scarp zone. These observations are consistent with previous studies by Walter & Joswig (2008, 2009) and Walter *et al.* (2011), who located fractures, fissures, and rock falls within the Super-Sauze landslide and in the scarp zone, with the same seismogram and spectrogram signatures as in our data. Unfortunately, we could not estimate the depth of the seismic events. Some events (e.g. slide quakes) may originate from the bulk of the landslide, probably at discontinuities between layers, such as the smooth surface we observed on the field at Valoria (Fig. 13). One small seismic array per landslide is clearly not enough to precisely locate seismic events, because an array aperture of 40 m is much smaller than the size of the landslide. Several arrays should be installed, near the identified clusters to better detect and locate seismic events. This should help to better discriminate the source mechanisms for each type of seismic signals.

Finally, we compared surface displacement rates with the rate of seismic events. We found that the main peaks of seismic activity coincide with accelerations of the slide. The correlation is positive and significant at Valoria, which had the largest velocity. At Super-Sauze, there is also a positive correlation in 2010 May, a period characterized by moderate velocity, but the correlation is not significant at the 95 per cent confidence level. Finally, no correlation is observed in 2009 October at Super-Sauze, the acquisition period with the slowest velocity.

Similarly, we also found a positive correlation between rate of seismic events and rainfall, but only for the 2010 May period at Super-Sauze, which had the more important precipitation. At Valoria, no rainfall occurred during the seismic acquisition. However, important rainfall (more than 50 mm in the preceding 10 d) occurred just before the seismic acquisition, which probably triggered the landslide reactivation. Other important meteorological factors include snowmelt, which was important during the 2010 May acquisition at Super-Sauze, but its effect is more difficult to analyse since we have no measure of snow cover. We found no influence of earthquakes on landslide dynamics, probably because seismic shaking was too small during the acquisition periods analysed in this work (Keefer 1984, 2002). A longer acquisition time would be needed to better understand the influence and rainfall and earthquakes on landslide dynamics, and to better understand the link between microseismic activity and landslide displacement.

ACKNOWLEDGEMENTS

This research was funded through the ANR Risk-Nat project 'SISCA: Système intégré de Surveillance de Crises de glissements de terrain' (2009–2011). We are warmly grateful to all the colleagues of Stuttgart (Institut für Geophysik Stuttgart, Germany) and Modena (Dipartimento di Scienze della Terra, Università degli Studi di Modena e Reggio Emilia, Italy) for their huge aid in the fields and their encouraging discussions. We thank the colleagues of the OMIV observatory (Observatoire Multidisciplinaire des Instabilités de Versants) and of the IHR equipment and management team (Imagerie Haute Résolution, Coutant *et al.* 2005), who provided the equipment and the support during the field campaigns. For the Valoria monitoring campaign, instruments belonging to the French national pool of portable seismic instruments Sismob-RESIF were used. We also acknowledge M. Zillmer, G. Herquel and E. Forte for their help in tomography acquisition and their keen attention in analysing the velocity model inversion, the two anonymous reviewers for their thorough reviews and D. Goron for the English improvements.

REFERENCES

Almendros, J., Ibáñez, J.M., Alguacil, G. & Del Pezzo, E., 1999. Array analysis using circular-wave-front geometry: an application to locate the nearby seismoc-volcanic source, *Geophys. J. Int.,* **136,** 159–170.

Amitrano, D., Grasso, J.R. & Senfaute, G., 2005. Seismic precursory patterns before a cliff collapse and critical-point phenomena, *Geophys. Res. Lett.,* **32**(8), 1–5.

Amitrano, D., Gaffet, S., Malet, J.-P. & Maquaire, O., 2007. Understanding mudslides through microseismic monitoring: the Super-Sauze (South-East French Alps) case study, *Bull. Soc. Géol. Fr.,* **178**(2), 149–157.

Arattano, M., 1999. On the use of seismic detectors as monitoring and warning systems for debris flows, *Nat. Haz.,* **20,** 197–213.

Arattano, M. & Marchi, L., 2005. Measurements of debris-flow velocity through cross-correlation of instrumentation data, *Nat. Haz. Earth Syst. Sci.,* **5,** 137–142.

Baldi, A.M., De Luca, J., Lucente, C. & Sartini, G., 2009. *Indagine di sismica a rifrazione per lo studio della frana attiva dei Boschi di Valoria. Atti del 3° Congresso Nazionale AIGA—Centro di GeoTecnologie,* Università degli Studi di Siena, san Giovanni Valdarno (AR), 25–27 Febbraio 2009, 33–34.

Borgatti, L., Corsini, A., Barbieri, M., Sartini, G., Truffelli, G., Caputo, G.E. & Pugliesi, C., 2005. Large reactivated landslides in weak rock masses: a case study from the Northern Apennines (Italy), *Landslides,* **3,** 115–124.

Brückl, E. & Mertl, S., 2006. Seismic monitoring of deep-seated mass movements, in *Proceedings of INTERPRAEVENT International Symposium "Disaster Mitigation of Debris Flows, Slope Failures and Landslides*," pp. 571–580, Universal Academy Press, Inc., Tokyo, Japan.

Bertacchini, E., Capitani, A., Capra, A., Castagnetti, C., Corsini, A., Dubbini, M. & Ronchetti, F., 2009. Integrated surveying system for landslide monitoring, Valoria Landslide (Apennines of Modena, Italy), in *Proceedings of FIG 2009, Surveyors Key Role in Accelerated Development,* Eilat, Israel, 3–8 May 2009 (on CD-ROM).

Burtin, A., Bollinger, L., Cattin, R., Vergne, J. & Nábělek, J.L., 2009. Spatiotemporal sequence of Himalayan debris flow from analysis of high-frequency seismic noise, *J. geophys. Res.,* **114,** 1–15.

Cadman, J.D. & Goodman, R.E., 1967. Landslide noise, *Science,* **158,** 1182–1184.

Cole, S.E., Cronin, S.J., Sherburn, S. & Manville, V., 2009. Seismic signals of snow-slurry lahars in motion: 25 September 2007, Mt. Ruapehu, New Zealand, *Geophys. Res. Lett.,* **36**(9), doi:10.1029/2009GL038030.

Corsini, A., Borgatti, L., Cervi, F., Dähne, A., Ronchetti, F. & Sterzai, P., 2009a. Estimating mass-wasting processes in active earth slides—earth flows with time-series of high-resolution DEMs from photogrammetry and airborne LIDAR, *Nat. Haz. Earth Syst. Sci.,* **9,** 433–439.

Corsini, A. *et al.*, 2009b. Monitoring meters-per-day active earthflows using Automated Total Station and Ground-Based SAR, in *Proceedings of FIST Geoitalia 2009 (CD-ROM)*.

Coutant, O., Doré, F., Fels, J.F., Brunel, D., Dietrich, M., Brenguier, F. & Judenherc, S., 2005. The High Resolution Seismic Imaging (IHR) network, a new tool for seismic investigations at hectometric scales, *Geophys. Res. Abstr.,* **7**.

Cusano, P., Damiano, N., Petrosino, S., Zaccarelli, L., Corsini, A., Borgatti, L., Cervi, F. & Ronchetti, F., 2006. Acquisizione di rumore sismico nell'Appenino Reggiano Modenese, Open File Report, 1–15 Aprile 2006.

Dammeier, F., Moore, J.R., Haslinger, F. & Loew, S., 2011. Characterization of alpine rockslides using statistical analysis of seismic signals, *J. geophys. Res.,* **116,** F04024, doi:10.1029/2011JF002037.

De Angelis, S., Bass, V., Hards, V. & Ryan, G., 2007. Seismic characterization of pyroclastic flow activity at Soufrière Hills Volcano, Montserrat, 8 January 2007, *Nat. Haz. Earth Syst. Sci.,* **7,** 467–472.

Deparis, J., Jongmans, D., Cotton, F., Baillet, L., Thouvenot, F. & Hantz, D., 2008. Analysis of rock-fall and rock-fall avalanche seismograms in the French Alps, *Bull. seism. Soc. Am.,* **98**(4), 1781–1796.

Déprez, A., Malet, J.-P., Ulrich, P., Masson, F., Lissak, C. & Maquaire, O., 2011. Continuous monitoring and near-real time processing of GPS observations for landslide analysis: a methodological framework, in *Proceedings of the Second World Landslide Forum,* eds Margottini, C., Canuti, P. & Sassa, K., 3–7 October 2011, Springer, Rome, Italy.

Esposito, A.M., Giudicepietro, F., Scarpetta, S., D'Auria, L., Marinaro, M. & Martini, M., 2006. Automatic discrimination among landslide, explosion-quake, and microtremor seismic signals at Stromboli Volcano using neural networks, *Bull. seism. Soc. Am.,* **96,** 1230–1240.

Garberi, M.L., Palumbo, A., Pizziolo, M., with the contribution of Baldelli, C., Barchiesi, P., Bertolini, G. & De Nardo, M.T., 1999. I numeri sulle frane, *Regione Emilia-Romagna,* Servizio Cartografico e Geologico, Bologna, Italy.

Ge, M., 2005. Efficient mine microseismic monitoring, *Int. J. Coal Geol.,* **64**(1), 44–56.

Gomberg, J., Schulz, W., Bodin, P. & Kean, J., 2011. Seismic and geodetic signatures of faults slip at the Slumgullion Landslide natural laboratory, *J. geophys. Res.,* **116,** B09404, doi:10.1029/2011JB008304.

Grandjean, G., Malet, J.-P., Bitri, A. & Méric, O., 2006. Geophysical data fusion by fuzzy logic for imaging the mechanical behaviour of mudslides, *Bull. Soc. Géol. Fr.,* **177**(2), 127–136.

Guzzetti, F., Peruccacci, S., Rossi, M. & Stark, C.P., 2007. Rainfall thresholds for the initiation of landslides in central and southern Europe, *Meteor. Atmos. Phys.,* **98,** 239–267.

Helmstetter, A. & Garambois, S., 2010. Seismic monitoring of Séchilienne Rockslide (French Alps): analysis of seismic signals and their correlation with rainfalls, *J. geophys. Res.,* **115,** F03016, doi:10.1029/2009JF001532.

Hibert, C., Mangeney, A., Grandjean, G. & Shapiro, N., 2011. Slope instabilities in Dolomieu crater, Reunion Island: from seismic signals to rockfall characteristics, *J. geophys. Res.,* **116,** F04032, doi:10.1029/2011JF002038.

Huang, C.-J., Shieh, C.-L. & Yin, H.-Y., 2004. Laboratory study of the underground sound generated by debris flows, *J. geophys. Res,* **109,** F01008, doi:10.1029/2003JF000048.

Husker, A., Peyrat, S., Shapiro, N. & Kostoglodov, V., 2010. Automatic non-volcanic tremor detection in the Mexican subduction zone, *Geofísica Int.,* **49**(1), 17–25.

Joswig, M., 2008. Nanoseismic monitoring fills the gap between microseismic network and passive seismic, *First Break,* **26,** 117–124.

Keefer, D.K., 1984. Landslides caused by earthquakes, *Geol. Soc. Am. Bull.,* **95,** 406–421.

Keefer, D.K., 2002. Investigating landslides caused by earthquakes—an historical review, *Surv. Geophys.,* **23,** 473–510.

Kishimura, K. & Izumi, K., 1997. Seismic signals induced by snow avalanche flow, *J. Nat. Haz.,* **15**(1), 89–100.

Lacroix, P. & Helmstetter, A., 2011. Location of seismic signals associated with microearthquakes and rockfalls on Séchilienne landslide, *Bull. seism. Soc. Am.,* **101**(1), 341–353.

Lacroix, P., Grasso, J.-R.J., Roulle, J., Giraud, G., Goetz, D., Morin, S. & Helmstetter, A., 2012. Monitoring of snow avalanches using a seismic array: location, speed estimation and relationships to meteorological variables, *J. geophys. Res.,* **117**(1), doi:10.1029/2011JF002106.

Lévy, C., Jongmans, D. & Baillet, L., 2011. Analysis of seismic signals recorded on a prone-to-fall rock column (Vercors massif, French Alps), *Geophys. J. Int.,* **186,** 296–310.

Mainsant, G., Larose, E., Brönnimann, C., Jongmans, D., Michoud, C. & Jaboyedoff, M., 2012. Ambient seismic noise monitoring of a clay landslide: toward failure prediction, *J. geophys. Res.,* **117,** doi:10.1029/2011JF002159.

Malet, J.-P., Maquaire, O. & Calais, E., 2002. The use of Global positioning system for the continuous monitoring of landslides, *Geomorphology,* **43,** 33–54.

Malet, J.-P., 2003. Les "glissements de type écoulement" dans les marnes noires des Alpes du Sud. Morphologie, fonctionnement et modélisation hydro-mécanique, *PhD thesis,* École et Observatoire des Sciences de la Terre, Université Louis Pasteur, Strasbourg.

Marchi, L., Arattano, M. & Deganutti, A.M., 2001. Ten years of debris-flow monitoring in the Moscardo Torrent (Italian Alps), *Geomorphology,* **46,** 1–17.

Maquaire, O., Malet, J.-P., Remaître, A., Locat, J., Klotz, S. & Guillon, J., 2003. Instability conditions of marly hillslopes, towards landsliding or gullying? The case of the Barcelonnette basin, South East France, *Eng. Geol.,* **70**(1–2), 109–130.

Méric, O., Garambois, S., Malet, J.-P., Cadet, H., Guéguen, P. & Jongmans, D., 2007. Seismic noise-based methods for soft-rock landslide characterisation, *Bull. Soc. Géol. Fr.,* **178**(2), 137–148.

Mourot, P., 2008. Méthodes et Outils pour l'Auscultation et la Surveillance des Instabilités Gravitaires, *Thèse de doctorat,* Laboratoire de Géophysique Interne et de Tectonophysique, Université de Savoie, Grenoble.

Novosad, S., Blaha, P. & Kneijzlik, J., 1977. Geoacoustic methods in the slope stability investigation, *Bull. Int. Assoc. Eng. Geology,* **16,** 228–231.

Ronchetti, F., Borgatti, L., Cervi, F., Lucente, C.C., Veneziano, M. & Corsini, A., 2007. The Valoria landslide reactivation in 2005–2006 (Northern Appenines, Italy), *Landslides,* **4**(2), 189–195.

Ronchetti, F., 2008. Caratteristiche idro-meccaniche di grandi frane per scivolamento-colata in ammassi rocciosi deboli ed eterogenei: analisi

e modellizzazione di casi di studio circostanti il Monte Modino (Alta Val Secchia, Appennino settentrionale), *Tesi per il conseguimento del titolo di Dottore di ricerca,* Università degli Studi di Modena e Reggio-Emilia.

Roth, M., Dietrich, M., Blikra, L.H. & Lecomte, I., 2005. Seismic monitoring of the unstable rock slope site at Åknes, Norway, NORSAR Report, Oslo.

Rouland, D., Legrand, D., Zhizhin, M. & Vergniolle, S., 2009. Automatic detection and discrimination of volcanic tremors and tectonic earthquakes: an application to Ambrym volcano, Vanuatu, *J. Volcanol. Geoth. Res.,* **181,** 196–206.

Rouse, C., Styles, P. & Wilson, S.A., 1991. Microseismic emissions from flowslide-type movements in South Wales, *Eng. Geol.,* **31,** 91–110.

Roux, P.F., Marsan, D., Métaxian, J.P., O'Brien, G. & Moreau, L., 2008. Microseismic activity within a serac zone in an alpine glacier (Glacier d'Argentière, Mont Blanc, France), *J. Glaciol.,* **54**(184).

Schädler, W., 2010. Slope movements of the earthflow type—Engineering-geological Investigation, Geotechnical Assessment and Modelling of the Source Areas on the Basis of Case Studies from the Alps and Apennines, *PhD thesis,* Naturwissenschaftlichen Fakultät der Friedrich-Alexander-Universität Erlangen-Nümberg.

Schneider, D., Bartelt, P., Caplan-Auerbach, J., Christen, M., Huggel, C. & McArdell, B.W., 2010. Insights into rock-ice avalanche dynamics by combined analysis of seismic recordings and a numerical avalanche model, *J. geophys. Res.,* **115,** F04026, doi:10.1029/2010JF001734.

Senfaute, G., Duperret, A. & Lawrence, J.A., 2009. Microseismic precursory cracks prior to rock-fall on coastal chalk cliffs: a case study at Mesnil-Val, Normandie, NW France, *Nat. Haz. Earth Syst. Sci.,* **9,** 1625–1641.

Sick, B., Walter, M. & Joswig, M., 2012. Visual event screening of continuous seismic data by super-sonograms, *Pure appl. Geophys.* [online], doi:10.1007/s00024-012-0618-x.

Spillmann, T., Maurer, H., Green, G.A., Heincke, B., Willenberg, H. & Husen, S., 2007. Microseismic investigation of an unstable mountain slope in the Swiss Alps, *J. geophys. Res.,* **112,** 1–25.

Sterzai, P. *et al.*, 2010. LIDAR and Hyperspectral data integration for landslide monitoring: the test case of Valoria landslide, *Ital. J. Remote Sens.,* **42**(3), 89–99.

Stuart, G., Murray, T., Brisbourne, A., Styles, P. & Toon, S., 2005. Seismic emissions from a surging glacier: Bakaninbreen, Svalbard, *Ann. Glaciol.,* **42,** 151–157.

Suriñach, E., Sabot, F., Furdada, G. & Vilaplana, J.M., 2000. Study of seismic signals of artificially released snow avalanches for monitoring purposes, *Phys. Chem. Earth (B),* **25,** 721–727.

Suriñach, E., Furdada, G., Sabot, F., Biescas, B. & Vilaplana, J.M., 2001. On the characterization of seismic signals generated by snow avalanches for monitoring purposes, *Ann. Glaciol.,* **32,** 268–274.

Thomas, A.M., Nadeau, R.M. & Bürgmann, R., 2009. Tremor-tide correlations and near lithostatic pore pressure on the deep San Andreas fault, *Nature,* **462,** doi:10.1038/nature08654.

Thouvenot, F., Fréhet, J., Guyoton, F., Guiguet, R. & Jenatton, L., 1990. Sismalp: an automatic phone-interrogated seismic network for the western Alps, *Cahiers du Centre Européen de Géodynamique et de Séismologie,* **1,** 1–10.

Travelletti, J., Oppikofer, T., Delacourt, C., Malet, J.-P. & Jafoyedoff, M., 2008. Monitoring landslide displacements during a controlled rain experiment using a long-range terrestrial laser scanning (TLS). International Archives of the Photogrammetry, Remote Sensing and Spatial Information Sciences 37, Part B5, Beijing 2008.

Travelletti, J., Delacourt, C., Allemand, P., Malet, J.-P., Schmittbuhl, J., Toussaint, R. & Bastard, M., 2011. Correlation of multi-temporal ground based optical images for landslide monitoring: application, potential and limitations, *Int. J. Photogr. Remote-Sens.,* **70,** 39–55.

Travelletti, J. & Malet, J.-P., 2012. Characterization of the 3D geometry of flow-like landslides: a methodology based on the integration of heterogeneous multi-source data, *Eng. Geol.,* **128,** 30–48.

Walter, M. & Joswig, M., 2008. Seismic monitoring of fracture processes generated by a creeping landslide in the Vorarlberg Alps, *First Break,* **26,** 131–135.

Walter, M. & Joswig, M., 2009. Seismic characterisation of slope dynamics caused by softrock-landslides: the Super-Sauze case study, in *Proceedings of the International Conference on Landslide Processes: from geomorpholgic mapping to dynamic modelling,* pp. 215–220, eds Malet, J.-P., Remaître, A. & Boogard, T.A., CERG Editions, Strasbourg.

Walter, M., Niethammer, U., Rothmund, S. & Joswig, M., 2009. Joint analysis of the Super-Sauze (French Alps) mudslide by nanoseismic monitoring and UAV-based remote sensing, *First Break,* **27,** 53–60.

Walter, M., Arnhardt, C. & Joswig, M., 2011. Seismic monitoring of rockfalls, slide quakes, and fissure development at the Super-Sauze mudslide, *Fr. Alps. Eng. Geol.,* **128,** 12–22.

Wang, H. & Ge, M., 2007. Acoustic emission/microseismic source location analysis for a limestone mine exhibiting high horizontal stresses, *Int. J. oRock Mech. Mining Sci.,* **45,** 720–728.

Weber, D., 1994. Research into earth movements in the Barcelonnette basin, in *Temporal Occurence and Forecasting of Landslides in the European Community,* Final Report, Vol. I, pp. 321–336, eds Casale, R., Fantechi, R. & Flageollet, J.C., Contract EPOCH, European Comission.

Wust-Bloch, G.H. & Joswig, M., 2006. Pre-collapse identification of sinkholes in unconsolidated media at Dead Sea area by "nanoseismic monitoring" (graphical jackknife location of weak sources by few, low-SNR records), *Geophys. J. Int,>* **167**(3), 1220–1232.

Yang, C., Luo, Z., Hu, G. & Liu, X., 2007. Application of a microseismic monitoring system in deep mining, *J. Uni. Sci. Technol. Beij.,* **14**(1), 6–8.

Zobin, V.M., Plascencia, I., Reyes, G. & Navarro, C., 2009. The characteristics of seismic signals produced by lahars and pyroclastic flows: volcán de Colima, México, *J. Volcanol. Geotherm. Res.,* **179,** 157–167.